Atmospheric
Chemistry
and Physics

Mass spectrometric analysis of unprecedented high levels of carbonaceous aerosol particles long-range transported from wildfires in the Siberian Arctic

Eric Schneider[1,2], **Hendryk Czech**[1], **Olga Popovicheva**[3], **Marina Chichaeva**[4], **Vasily Kobelev**[4], **Nikolay Kasimov**[4], **Tatiana Minkina**[5], **Christopher Paul Rüger**[1,2], and **Ralf Zimmermann**[1,2]

[1]Joint Mass Spectrometry Centre (JMSC), Chair of Analytical Chemistry,
University of Rostock, 18059 Rostock, Germany
[2]Department of Life, Light & Matter (LLM), University of Rostock, 18059 Rostock, Germany
[3]Skobeltsyn Institute of Nuclear Physics, Lomonosov Moscow State University,
Leninskie Gory, 1, 119991 Moscow, Russia
[4]Faculty of Geography, Lomonosov Moscow State University, Leninskie Gory, 1, 119991 Moscow, Russia
[5]Academy of Biology and Biotechnology, Southern Federal University, 344090 Rostov-on-Don, Russia

Correspondence: Hendryk Czech (hendryk.czech@uni-rostock.de)

Abstract. Wildfires in Siberia generate large amounts of aerosols, which may be transported over long distances and pose a threat to the sensitive ecosystem of the Arctic. Particulate matter (PM) of aged wildfire plumes originating from Yakutia in August 2021 was collected in Nadym and on Bely Island (both in northwestern Siberia). An advanced analysis of the chemical composition of aerosol particles was conducted through a multi-wavelength thermal–optical carbon analyzer (TOCA) coupled to resonance-enhanced multiphoton ionization time-of-flight mass spectrometry (REMPI-TOFMS) as well as through ultra-high-resolution Fourier-transform ion cyclotron resonance mass spectrometry (FT-ICR MS). In Nadym, concentrations of organic carbon (OC) and elemental carbon (EC) peaked at 100 and $40\,\mu g\,m^{-3}$, respectively, associated with Angström absorption exponents for 405 and 808 nm ($AAE_{405/808}$) between 1.5 and 3.3. The weekly average on Bely Island peaked at $8.9\,\mu g\,m^{-3}$ of OC and $0.3\,\mu g\,m^{-3}$ of EC and $AAE_{405/808}$ close to unity. In particular, ambient aerosol in Nadym had a distinct biomass burning profile with pyrolysis products from carbohydrates, such as cellulose and hemicellulose, as well as lignin and resinoic acids. However, temporarily higher concentrations of five- and six-ring polycyclic aromatic hydrocarbons (PAHs), different from the PAH signature of biomass burning, suggest a contribution of regional gas flaring. FT-ICR MS with electrospray ionization (ESI) revealed a complex mixture of highly functionalized compounds, containing up to 20 oxygen atoms, as well as nitrogen- and sulfur-containing moieties. Concentrations of biomass burning markers on Bely Island were substantially lower than in Nadym, flanked by the appearance of unique compounds with higher oxygen content, higher molecular weight, and lower aromaticity. Back-trajectory analysis and satellite-derived aerosol optical depth suggested long-range transport of aerosol from the center of a Yakutian wildfire plume to Nadym and from the plume periphery to Bely Island. Owing to lower aerosol concentrations in the plume periphery than in its center, it is demonstrated how dilution affects the chemical plume composition during atmospheric aging.

1 Introduction

The Arctic is a particularly vulnerable region regarding the effects of global warming, with atmospheric temperatures increasing at 2 to 3 times the global average rate; this phenomenon is referred to as Arctic amplification (IPCC, 2013; Schmale et al., 2021). In addition to carbon dioxide and other greenhouse gases, particulate matter (PM) emissions transported to the Arctic region also contribute to the rapid warming. Black carbon (BC) is emitted by fossil fuel combustion and biomass burning and is linked to the light absorption of the atmosphere as well as of snow or ice surfaces. Long-range transport to the Arctic carries BC and other tracers of anthropogenic and wildfire origin (Bond et al., 2013; Manousakas et al., 2022; Matsui et al., 2022; Moschos et al., 2022; Stohl et al., 2013). Beyond BC, wildfires are a major source of volatile organic compounds (VOCs), primary organic aerosol (POA), and brown carbon (BrC), which can act as a strong absorber of solar radiation at ultraviolet (UV) and visible wavelengths (Farley et al., 2022; Forrister et al., 2015; Fleming et al., 2020).

The frequency and size of wildfire events have increased during recent decades, and the trend is expected to continue due to global warming and the associated rise in extreme weather events (Abatzoglou et al., 2019; Kharuk et al., 2021). As wildfires in the northern regions increase, the long-range transport of wildfire plumes from central Siberia to Arctic regions can become more common, increasing the impact of carbonaceous aerosols in the Arctic on radiative forcing (Calì Quaglia et al., 2022; Yue et al., 2022). Siberian wildfire plumes may even reach densely populated regions in Europe or East Asia (Ikeda and Tanimoto, 2015; Semoutnikova et al., 2018); this is associated with a significantly increased risk of mortality as well as respiratory and cardiovascular diseases of the exposed population (Chen et al., 2021). Although northern boreal regions like Siberia are predicted to be impacted the most by increasing wildfire intensity, studies investigating organic aerosol emissions, especially from Siberia, are scarce (Flannigan et al., 2009).

In addition to individual fuel properties, combustion conditions largely affect the emission composition. Low combustion efficiency with a flameless burning (smoldering) generates aerosols rich in organic matter (OM) (Kalogridis et al., 2018), resembling the composition of the biomass by intense release of phenolic building blocks from lignin, cellulose, and hemicellulose (Simoneit, 2002) and containing tar-like BrC with Angström absorption exponents (AAEs) significantly larger than unity (Chakrabarty et al., 2010). Under flaming conditions, the overall organic aerosol content is reduced; soot carbon, related to elemental carbon (EC), and parent polycyclic aromatic hydrocarbons (PAHs) become more substantial aerosol constituents; and the AAE shifts to unity (Popovicheva et al., 2016, 2015).

Atmospheric aging reactions under the influence of, e.g., UV radiation, ozone, NO_x, or SO_x, transform organic vapors and OM by, e.g., photolysis and hydroxyl and nitrate radical reactions (Peng et al., 2021; Surratt et al., 2008; Forrister et al., 2015). In homogeneous gas-phase reactions, organic vapors may be oxidized and condense as secondary organic aerosol (SOA) on existing particles or even form new particles (nucleation). Moreover, heterogeneous reactions between atmospheric oxidants and particle constituents may increase the molecular complexity of primary aerosols in the atmosphere, which is associated with higher functionalization, an increase in heteroatom content (O, N, S), and oligomer formation. Additionally, reactions between individual constituents of the particle phase complete the ongoing complex multiphase chemistry (Schneider et al., 2022; Pardo et al., 2022; Lin et al., 2015; Chacon-Madrid and Donahue, 2011). For biomass burning, atmospheric aging may promote the formation of chromophores and thus BrC but may also lead to a degradation of chromophores by photochemistry with increasing atmospheric lifetime (Fleming et al., 2020; Forrister et al., 2015).

Wildfires may rapidly increase the level of particulate matter (PM) to a range that atmospheric oxidant concentrations become insufficient to uniformly process the wildfire aerosol, leading to differences in atmospheric processing of plume centers and the plume periphery (Hodshire et al., 2021). For example, OH radicals, the main oxidant under photochemical conditions, may already be consumed at the periphery of the plume, so enhanced photobleaching was observed at the plume edges relative to the core (Lee et al., 2020), along with faster photochemistry (Palm et al., 2021). Furthermore, other photosensitive atmospheric oxidants, such as NO_3 radicals, may be protected by the plume optical depth and become relevant for the chemistry in the plume center (Decker et al., 2021). Consequently, the product spectrum of atmospheric processing differs from aging of biomass burning aerosol at typical ambient conditions. Additionally, the net appearance of OM in wildfire plumes during aging becomes dilution driven as high near-source aerosol concentrations release adsorbed and absorbed vapors during atmospheric transport (Palm et al., 2020), on the one hand counteracting the known significant net increase of OM mass for a wide range of biomass burning aerosol aging (Ortega et al., 2013) but on the other hand forming secondary organic aerosol (Fang et al., 2021; Li et al., 2020). As aerosol concentrations at the plume periphery are lower than in the center, they undergo more intense aging (Hodshire et al., 2021). Quantification of transported wildfire aerosol and its molecular characterization during aging may improve the understanding of the impacts on the sensitive Arctic ecosystem and related effects on climate.

Siberian wildfires are a major source of climate-relevant species emitted at northern latitudes (Lavoué et al., 2000). Yakutia in eastern Siberia is known to be prone to large-scale wildfires (Tomshin and Solovyev, 2018) owing to the combination of hot summers with temperatures up to 40 °C; low humidity in the atmosphere and pedosphere;

and the phenomenon of dry thunderstorms, which have been estimated to account for more than half of the fire causes. As such, lightning ignites dry biomass, while strong wind accelerate the spread of the fire (Narita et al., 2021). On 4 August 2021, strong smoke enveloped large areas of western Siberia, namely Yamalo-Nenets Autonomous Okrug (YNAO) and Khanty-Mansysky Autonomous Okrug (KMAO) (NUR24.RU, 2021).

In our study, intensively high concentrations of OC and EC were observed in Nadym and on Bely Island, located in the north of western Siberia, during August 2021, according to filter samples collected at both locations. Backward air mass trajectories and satellite images indicated large-scale wildfires in Yakutia as the main source. Multi-wavelength thermal–optical carbon analysis with photoionization mass spectrometry and ultra-high-resolution mass spectrometry with complementary ionization techniques confirm the origin of the observed high OC and EC concentrations and provide an advanced chemical characterization of Arctic pollution associated with aerosol emissions from vast Siberian fires and differences in atmospheric aging of the plume center and plume periphery.

2 Experimental section

2.1 Sampling sites

One part of the sampling campaign was carried out in Nadym from 5 to 12 August 2021. A total suspended particle (TSP) sampling system was operated in an area far from roads and residential sectors, with a flow rate of $70 \, \mathrm{L \, min^{-1}}$ and variable duration of 3–12 h to achieve comparable filter loadings of the nine resulting samples. Quartz fiber filters (QFFs; 47 mm, QM-A 1851047, Whatman, USA) were used to collect PM samples, after 6 h of pretreatment at $600 \, ^\circ \mathrm{C}$.

The second sampling system was operated at the pavilion of the research aerosol station Island Bely installed for the purpose of addressing pollution in the western Siberian Arctic (Popovicheva et al., 2023, 2022). The TSP inlet was installed approximately 1.5 m above the roof and 4 m above the ground for filter sampling (see Popovicheva et al., 2022, for details). Three QFFs were collected by weekly sampling, starting on 31 July 2021 and ending on 21 August 2021, with a sampling flow rate of $2.3 \, \mathrm{m^{-3} \, h^{-1}}$. A more detailed overview of the sampling parameters as well as an in-depth discussion of the study area and typical PM emissions sources can be found in Sect. S1 in the Supplement.

2.2 Air mass transportation

To evaluate the impact of air mass transportation and smoke plume origin, 240 h backward trajectories (BWTs) were generated using the NOAA HYSPLIT model of the Air Resources Laboratory (Stein et al., 2015) and archive data from the National Center for Environmental Prediction's Global

Data Assimilation System with the coordinate resolution equal to $1^\circ \times 1^\circ$ latitude and longitude and an input height of 500 m above ground. Additional BWT calculations with input heights of 10, 100, 250, and 500 m are presented in Fig. S1.

Data on the occurrence of fires were obtained from the Fire Information for Resource Management System (FIRMS) operated by NASA's Earth Science Data and Information System (ESDIS) (https://firms.modaps.eosdis.nasa.gov/map, last access: 3 April 2023) at GSFC based on satellite observations which register open flaming. This work uses data arrays on the spatial location of fire centers from the Moderate Resolution Imaging Spectroradiometer (MODIS). The satellite images of smoke plumes in the sampling days were obtained from https://worldview.earthdata.nasa.gov (last access: 3 April 2023). Fire activity is shown in 10 d back from a day of BWT analyses (Fig. 2).

The Ozone Mapping and Profiling Suite (OMPS) aerosol index information was obtained from the Goddard Earth Sciences Data and Information Services Center (GES DISC) based on satellite instrumentation that measures the radiance scattered by the limb of the atmosphere. The OMPS aerosol index is based on the normalized radiance of the 340 and 378.5 nm wavelengths (Torres, 2019).

2.3 Analytical instrumentation

2.3.1 Fourier-transform ion cyclotron resonance mass spectrometry (FT-ICR MS)

Ultra-high-resolution FT-ICR MS measurements were carried out on a solariX (Bruker Daltonik, Bremen, Germany) equipped with a 7 T superconducting magnet and an InfinityCell$^\copyright$. A detailed description of the extraction procedure as well as the settings for each ionization technique can be found in Sect. S2. Shortly, filter extracts were analyzed in positive and negative mode electrospray ionization (ESI), as well as positive-mode atmospheric pressure photoionization (APPI; Kr, 10/10.6 eV) with a direct-infusion ion source setup (Bruker Daltonik, API ion source). For each measurement, 400 scans were collected in the range of m/z 150–1000 with a resulting resolving power $> 310\,000$ at m/z 400 and mass accuracy below 1 ppm.

2.3.2 Multi-wavelength thermal–optical carbon analysis coupled to resonance-enhanced multiphoton ionization time-of-flight mass spectrometry (TOCA-REMPI-TOFMS)

For direct analysis of filter samples, a thermal–optical carbon analyzer (TOCA; Model 2001, DRI, US) coupled to time-of-flight mass spectrometry (TOFMS) was used with resonance-enhanced multiphoton ionization (REMPI). Organic and elemental carbon (OC, EC) were determined according to the IMPROVE_A protocol (Chow et al., 2007) for the separation of pyrolytic OC from EC. Precisions of the carbon anal-

ysis are sample dependent and range between 2 % and 6 % for TC and 5 % and 10 % of the split between OC and EC, according to the manufacturer. In addition to 635 nm, the TOCA was further retrofitted with six laser diodes, emitting light in the visible UV and near-infrared (NIR) spectral range at 405, 445, 532, 780, 808, and 980 nm (Chen et al., 2015). The multi-wavelength TOCA was used to determine the Angström absorption exponent (AAE), which is defined for a wavelength pair λ_1/λ_2 by

$$AAE(ATN\lambda) = -\frac{\ln \frac{ATN_1}{ATN_2}}{\ln \frac{\lambda_2}{\lambda_1}} \tag{1}$$

with ATN being the light attenuation.

In this study, the wavelength pair of 405 and 808 nm was used to calculate the AAE ($AAE_{405/808}$), representing the exclusive absorption of BC in NIR and the lower visible UV range with absorption of both BrC and BC. ATN was derived from the ratio of the laser transmittance (LT) of the untreated filter sample before TOCA to the LT at the end of the TOCA so that refractive particle constituents are still retained. In order to account for filter loading effects on ATN, the empirical correction from Chow et al. (2021) was applied. The uncertainty of the AAE determination was derived from error propagation of the LT measurement, which has a precision of 8 % at 405 and 808 nm (Chen et al., 2015). Thus, the final uncertainty of the $AAE_{405/808}$ calculation is within $\pm 15\%$ at 95 % confidence.

A small fraction of evolving particulate matter during IMPROVE_A is bypassed from the carbon quantification by a modified quartz tubing behind the oven of the TOCA and reaches a REMPI-TOF-MS through a heated transfer capillary (Grabowsky et al., 2011). REMPI refers to a selective ionization technique for aromatic compounds and predominantly yields molecular ions (Streibel and Zimmermann, 2014). A more detailed description of REMPI can be found in Sect. S2.3.

2.4   Mass spectrometric and statistical data analysis

External mass calibration of the FT-ICR MS was performed using arginine oligomers covering the entire mass range. An internal calibration of each mass spectrum was performed by characteristic and commonly abundant peaks from a self-generated calibration list (CHO_x and $CHNO_x$ class compounds, manually verified), achieving sub-parts per million mass accuracies. Raw data were peak picked (cutoff: S/N = 6) and exported with Bruker Data Analysis 5.1 (Bruker Daltonik, Bremen, Germany). The exported mass spectra were processed by self-written MATLAB algorithms and routines combined in a graphical user interface named CERES Processing (Rüger et al., 2017). After careful investigation and taking into account attribution boundaries from the literature, the following restrictions were deployed for elemental composition assignment in the range of

150–1000 m/z: $C_cH_hN_nO_oS_sNa_{na}$; $5 \leq c \leq 60$, $5 \leq h \leq 100$, $n \leq 3$, $o \leq 20$, $s \leq 1$ (ESI+: na ≤ 1) with a maximum error of 1 ppm (Tang et al., 2020; Schneider et al., 2022). Additional restrictions were applied for the H/C ratio (0.4–2.4), O/C ratio (0–1.4), and double-bond equivalents (DBEs; 0–28). The assignment of radical cations was allowed for APPI. Equations used for the calculation of molecular properties can be found in Sect. S2.4.

Principal component analysis (PCA) and hierarchical cluster analysis (HCA) were performed by the MATLAB R2021b Statistics Toolbox (MathWorks, Inc., MA). HCA was performed with the following settings: unweighted average distance (UPGMA), cosine distance metric, maximum number of clusters set to five, and absolute intensities normalized by power transformation. Prior to PCA, sum parameters were standardized to a mean of 0 and standard deviation of 1.
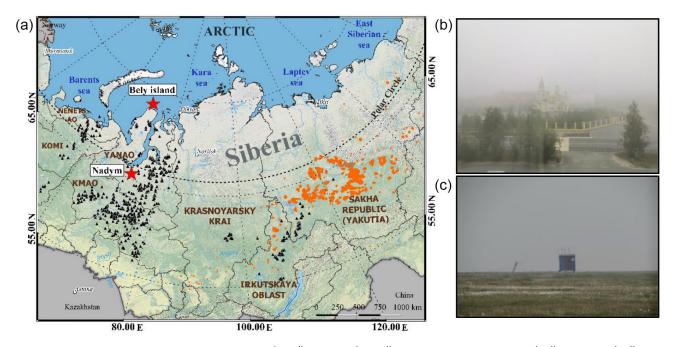
Calculation of relative sum formula intensities is done by the L1 norm (normalization to total ion current, TIC) of all assigned elemental compositions of the respective sample.

3   Results and discussion

3.1   Air mass transportation to Nadym and Bely Island

Figures 2 and S2 present backward trajectories (BWTs) for air mass transport at times corresponding to sample collection in Nadym and on Bely Island throughout the sampling campaigns using the HYSPLIT simulation data. We present this analysis first, as it provides useful information for analysis of aerosol chemistry discussed in later sections. Extremely high smoke intensity was initially observed in Nadym on 5–6 August 2021 when samples N01 and N02 were collected (Table S1). Air masses that arrived on those days in Nadym from the NE and NNE directions passed the wildfire areas in Krasnoyarsk Krai (Figs. 1, S2, and S3). As observed from satellite images, they brought a wide and dense smoke plume that covered YNAO, KMAO, Yakutia, Krasnoyarsk Krai, and Irkutsk Oblast. On 7 August 2021 when samples N03, N04, and N05 were collected, BWTs arrived in Nadym from the NE direction. Subsequently, they passed through Yakutia, which had the largest density of detected fires, then Irkutsk Oblast and Krasnoyarsk Krai, before turning to YNAO (Fig. 2).

On 8 August 2021, the smoke plume area narrowed and almost localized over the territory of Krasnoyarsk Krai. When samples N07 and N08 were collected, the OMPS aerosol index in Nadym had declined from > 5 to < 0.625. Finally, air masses changed their direction, and on 9 August 2021 they arrived in Nadym from the NW and NNW. They brought clean Arctic air with an OMPS aerosol index below 0.625 from the White, Barents, and Kara seas. The clean Arctic background for BC was previously determined from the 20th percentile of 1.5 years of continuous monitoring, which accounted for $10 \, ng \, m^{-3}$. Background pollutant concentrations in Arctic stations are generally very low without any

Figure 1. Location of Bely Island $(73°20'7.57''\,N,\ 70°4'49.05''\,E)$ and Nadym $(65°32'00''\,N,\ 72°31'00''\,E)$ in Yamalo-Nenets Autonomous Okrug (YNAO) (western Siberia) (**a**). The map was created using the open-source geographic information system QGIS (https://qgis.org/en/site, last access: 3 April 2023) with ESRI physical imagery (https://server.arcgiso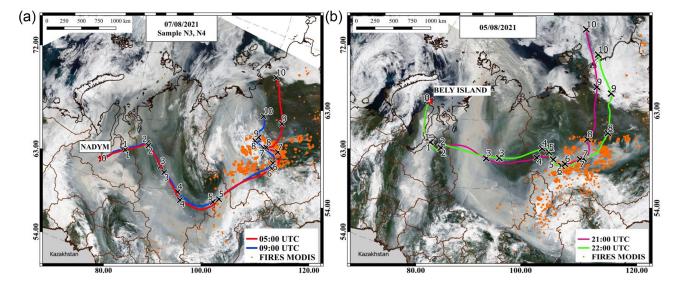nline.com/ArcGIS/rest/services/World_Physical_Map/MapServer/tile/%7Bz%7D/%7By%7D/%7Bx%7D&zmax=20&zmin=0, last access: 3 April 2023) as the base layer. Moreover, the open-source Natural_Earth_quick_start package was used to add a layer of natural and cultural boundaries and polygons from ESRI shapefile storage. VIIRS and MODIS active fire data for August 2021 have been downloaded from https://firms.modaps.eosdis.nasa.gov/ (last access: 3 April 2023), shown in orange. Flares of oil and gas fields are indicated for 2020 as black triangles (https://skytruth.org/, last update 2023). Photo of Nadym (**b**; https://nur24.ru/news/ecologia/smog-ot-pozharov-v-yakutii-polnostyu-okutal-yamal-foto-video, last access: 3 April 2023) and Island Bely station during the smoke event (**c**; photo taken by the authors).

detectable influence from local or regional sources (Eleftheriadis et al., 2004; Popovicheva et al., 2019). Conversely, episodes of pollution were defined by the 80th percentile, accounting for $90\,\mathrm{ng\,m^{-3}}$ (Popovicheva et al., 2022).

Air mass trajectories and satellite images reveal that the wildfire plume that has strongly impacted Nadym also reached further north into the Arctic and brought deep smoke into Bely Island during the same period from 5 to 7 August 2021. In contrast to the plume arriving in Nadym, the northern part of the evolving wildfire plume was first transported north from its origin for several days and moved around over the Arctic Ocean before a change in wind direction transported the plume westward. The OMPS aerosol index (Fig. S3) suggests that the periphery (lower OMPS aerosol index, approx. 1.85, yellow) of the Yakutian wildfire plume was transported to Bely Island, in contrast to the plume center aerosol transported to Nadym (higher OMPS aerosol index, > 5, red). This may have led to a gradient in photochemical processing of the plume, i.e., a lower extent of atmospheric processing by OH radicals, with the northern section containing more atmospherically aged aerosol and the south-

ern section more fresh wildfire emissions, which were picked up on the way westward.

3.2 Carbonaceous aerosol in Nadym and on Bely Island

Long-range transport of a wildfire plume from Yakutia caused high carbon concentrations in ambient PM in Nadym from 5 to 7 August 2021 (samples N01–N07) (Fig. 3). For sample N04, concentrations of organic carbon (OC) and elemental carbon (EC) approached a maximum of 100 and $40\,\mathrm{\mu g\,m^{-3}}$, respectively (Table S1). On 8 August 2021, OC and EC dropped to 5.4 and $1.7\,\mathrm{\mu g\,m^{-3}}$ for sample N08, respectively. On 9 August 2021 transport of clean Arctic air masses decreased OC and EC down to $0.7\,\mathrm{\mu g\,m^{-3}}$ and $0.1\,\mathrm{\mu g\,m^{-3}}$ for N09, respectively, while on 12 August 2021, $3.7\,\mathrm{\mu g\,m^{-3}}$ of OC and $1.2\,\mathrm{\mu g\,m^{-3}}$ of EC were obtained for N10 (Fig. 3). Regarding the distribution of the individual carbon fractions, no significant difference between the samples could be determined apart from a significantly higher contribution of EC2 in sample N10 (two-sided Grubbs test, significance level of 0.05), collected when smoke has almost disappeared (Table S1). EC2 has been associated with soot particles from internal combustion engines and indicates that

Figure 2. Backward trajectories with indications of transport time (days back indicated by crosses) and satellite images of smoke plume on the day of peaking concentrations of carbonaceous aerosols in Nadym on 7 August 2021 **(a)** and on Bely Island on 5 August 2021 **(b)**. The dates of sample completion for N03 and N04 from Nadym and B01 from Bely Island are presented. The maps were created using the open-source geographic information system QGIS (https://qgis.org/en/site, last access: 3 April 2023) with satellite imagery from 7 and 8 August 2021 (https://worldview.earthdata.nasa.gov, last access: 3 April 2023) with the TERRA MODIS fire anomaly layer and the MODIS-corrected reflectance true color imagery as the base layer (MODIS Science Team, 2017d, c, b, a). The open-source Natural_Earth_quick_start package was used to add a layer of natural and cultural boundaries and polygons from ESRI shapefile storage. Backward trajectories were calculated using HYSPLIT software (https://www.ready.noaa.gov/HYSPLIT.php, last access: 3 April 2023).
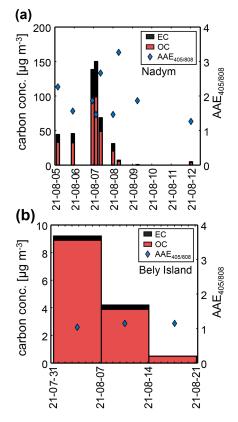
local emissions, e.g., from road traffic, contributed significantly to the carbonaceous aerosol. A generally substantial contribution of pyrolytic OC (OC_{pyro}) is an indication of the presence of biomass burning (BB) and secondary organic aerosol (SOA) (Grabowsky et al., 2011; Cheng et al., 2011).

In the week from 31 July 2021 to 6 August 2021 (sample B01, Bely Island) when the wildfire plume arrived in Nadym, concentrations of OC and EC at Bely Island reached the highest weekly averages of 8.9 and 0.3 $\mu g\,m^{-3}$, respectively, and declined in 2 subsequent weeks to 3.9 (B02) and 0.5 $\mu g\,m^{-3}$ (B03) of OC and 0.3 (B02) and $< 0.05 \mu g\,m^{-3}$ (B03) of EC (Table S1). PM of Bely Island was substantially affected by the wildfire emissions in Yakutia (Fig. 2), as was Nadym, but lower concentrations of carbonaceous aerosol particles were observed as only the periphery of the plume with lower aerosol concentrations was transported to Bely Island (Fig. S3).

The wavelength dependence of light absorption in the UV–Vis to near-infrared range is described by the AAE. While BC shows an AAE close to unity, BrC has a stronger increase in absorption towards lower wavelengths in the visible and UV range with AAE significantly larger than unity (Andreae and Gelencsér, 2006). Regarding biomass burning, spectral absorption obtained throughout the near-ultraviolet to near-infrared spectral region and high Angström absorption exponents (AAEs) up to 4.4 are found for smoke from smoldering combustion of pine debris in the wavelength regions from 370 to 670 nm. In contrast, open flaming smoke

from pine combustion shows a low AAE of around 1, also typical for high-temperature fossil fuel combustion, while mixed fires emit particles absorbing light with the intermediate AAE characteristics (Popovicheva and Kozlov, 2020).

For N01–N05, AAEs for the wavelength pair of 405 and 808 nm ($AAE_{405/808}$) were observed in the range of 1.5 to 3.3 (Fig. 3), showing the presence of significant amounts of BrC. Although there was no distinct relation of $AAE_{405/808}$ to concentrations of OC or EC, a moderate correlation coefficient of 0.59 was obtained between $AAE_{405/808}$ and the ratio of OC to EC (Fig. S4). This correlation indicates the contribution of aerosols from smoldering biomass burning, which is known to result in lower amounts of EC and BC but higher releases of BrC than flaming biomass burning (Cheng et al., 2011; Chen et al., 2006; Popovicheva et al., 2016). For N09, a moderately high $AAE_{405/808}$ of 1.9 was observed, which may be caused by a still-significant relative biomass burning contribution to overall low OC and EC concentrations. After the wildfire plume left Nadym, the lowest $AAE_{405/808}$ of 1.3 (N10) among all samples from Nadym was observed, pointing towards dominating aerosol emissions from fossil fuel combustion associated with a higher contribution of BC (Helin et al., 2021).

At Bely Island, the weekly average of $AAE_{405/808}$ of 1.0 for sample B01 (31 July to 6 August 2021) was not affected by BrC in the wildfire plume during the highest concentrations of OC and EC. In the subsequent 2 weeks with lower OC and EC concentrations, an $AAE_{405/808}$ of 1.2 was ob-

Figure 3. Carbon concentrations and Angström absorption exponent ($AAE_{405/808\,nm}$) in Nadym (a) and on Bely Island (b) measured by a multi-wavelength thermal–optical carbon analyzer (TOCA). Sampling conditions as well as EC and OC values, divided into individual fractions based on the IMPROVE_A protocol, are listed in Table S1.

tained, which is, however, not significantly different from 1 considering the associated measurement uncertainty of ± 0.5. Since lower aerosol concentrations from the periphery of the Yakutian wildfire plume reached Bely Island, it can be assumed that the wildfire aerosol has been more intensively processed during atmospheric transportation. Atmospheric aging may form BrC (Al-Abadleh, 2021), but, particularly toward longer photochemical ages, the phenomenon of photobleaching and whitening of BrC by atmospheric oxidants becomes dominant, decomposing chromophores and consequently decreasing AAE (Fang et al., 2021; Schnitzler et al., 2022) caused by a higher ratio of atmospheric oxidants to BB aerosols.
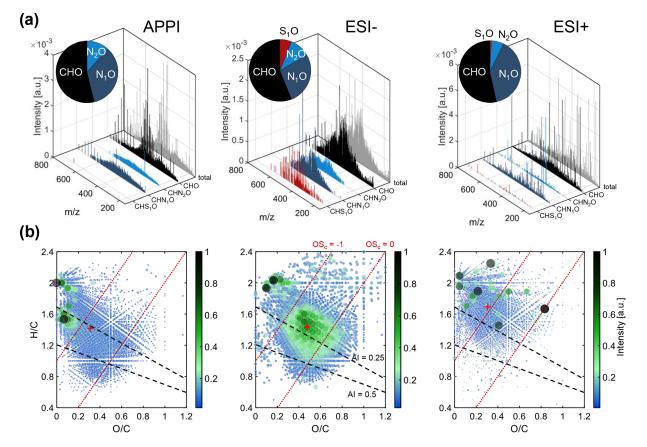
In Salekhard approximately 350 km west from Nadym and 800 km south from Bely Island, equivalent black carbon (eBC) was continuously measured during the summer of 2018, revealing an average concentration of $(350 \pm 120)\,ng\,m^{-3}$ (Popovicheva et al., 2020). Although EC and BC are determined by different measurement principles, they are highly correlated, appear in a similar concentration range, and essentially represent graphitized carbon (Wat-

son and Chow, 2002; Andreae and Gelencsér, 2006; Chow et al., 2021), thus enabling inter-comparison estimates. The observed concentrations of EC in Nadym during 5 to 7 August 2021 exceeded the BC concentrations in Salekhard by 2 orders of magnitude. Furthermore, even compared to the highest average levels for July and August from 2003 to 2017 of fine particulate matter ($PM_{2.5}$), primary OM, and BC caused by transported wildfire aerosol to YNAO (Yasunari et al., 2021), carbonaceous aerosol concentrations observed in Nadym in our study remain significantly high. At Bely Island, 10 times higher concentrations of OC and EC were observed compared to averages of organic aerosol and BC during summertime (Moschos et al., 2022; Popovicheva et al., 2022). Therefore, our results indicate unprecedented high concentrations of long-range-transported wildfire aerosol to the Arctic with different aging conditions between the two sampling sites.

3.3 PM bulk composition by APPI and ESI FT-ICR MS

All filter sample extracts analyzed by FT-ICR MS were measured with three atmospheric pressure ionization techniques: ESI+, ESI−, and APPI (+). A detailed discussion of the selectivity and sensitivity of each ionization technique can be found in Sect. S3.

Principal component analysis (PCA) based on FT-ICR MS average elemental compositions as well as other sum parameters, e.g., DBE, AI, H/C, and O/C (Table S3, Fig. S6), shows a clear grouping of samples N01 to N02 and N03 to N05 with a divergence of N07 and strong separation of N08 to N10. For chemical comparison of the FT-ICR MS data, samples are combined and classified based on the PCA results, previously discussed air mass trajectories, and the EC and OC concentrations. For Nadym, samples N01 to N05 are combined to form one dataset representing the strongest wildfire plume impact causing high OC and EC concentrations (Figs. 3 and S2). In contrast, samples N08 to N10 had the lowest concentrations of OC and EC. N09 was chosen as a reference for the absence of a wildfire impact, termed "ambient aerosol" for Nadym. The apparently different chemical composition of sample N07, indicating the influence of regional gas flaring, is separately addressed in Sect. 3.6. For Bely Island, sample B01 is selected for comparison with the Nadym dataset, as it represents the strongest wildfire impact at this location and additionally covers a similar time period (31 July to 7 August 2021) to the Nadym wildfire-plume-impacted samples (N01 to N05, 5 to 7 August 2021). Samples B02 and B03 represent a declining wildfire aerosol influence and ambient aerosol at Bely Island, respectively.

For the wildfire-plume-impacted samples (N01–N05), 1108 compounds are common between all ionization techniques (Fig. S5), but most compounds are uniquely identified by a single ionization technique. Notably, ESI+ and APPI share the highest number of common elemental compositions (1361), while ESI+ and ESI− share the lowest number (553)

Figure 4. FT-ICR MS data overview. **(a)** Averaged and normalized assigned elemental composition mass spectra of wildfire-plume-impacted samples in Nadym (N01–N05) in three ionization techniques (left to right: APPI, ESI−, and ESI+), with inserts of relative abundance pie charts of the four main compound classes. **(b)** Van Krevelen diagrams with average-intensity-weighted H/C and O/C ratios marked in red. The dotted lines indicate the limits of the average carbon oxidation state (OS_C; red) and modified aromaticity index (AI; black).
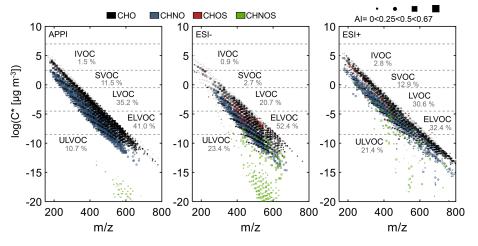
of two ionization techniques. In general, almost every compound detected in any ionization mode is part of a homologous series spanning several CH_2 units in the range of often 20 or more carbon atoms (Fig. S7). Other homologous series, including, e.g., methoxy groups, are also observed. The Van Krevelen diagrams (Fig. 4b) show complex fingerprints, with changing highest-intensity regions for each ionization technique. The lipid region (H/C > 2, low O/C, low aromaticity, low carbon oxidation state) is highly abundant, as well as lignin-like structures (medium H/C, medium O/C, AI < 0.5, and OS_C 0 to −1). In ESI, highly oxidized compounds with sugar-like structures (high O/C, low aromaticity, high OS_C) and highly oxidized molecules with high unsaturation (HU-HOMs) are observed additionally. This highlights the need for different ionization techniques to achieve a broad coverage of the chemical space, as has been shown before, e.g., for biomass burning tar balls from wildfires (Brege et al., 2021).

Saturation vapor pressure is a parameter used to characterize SOA (Donahue et al., 2011, 2012). Observed compounds in the wildfire plume show low to very low volatility as a result of high oxygen contents, and other heteroelements (N, S), gained by atmospheric aging during long-range transport

or maintained due to reduced photochemical processing. The majority of compounds is found in the low- to ultra-low-volatility area, but there is a difference when comparing individual compound classes.

3.4 Compound class characterization of PM in Nadym

3.4.1 CHO

Mass spectra of identified elemental compositions (Fig. 4a) show a broad distribution over the whole mass range (approx. 200–800 Da) of the highest abundant (rel. intensity) compound class. The relative intensity distribution of the oxygen number shows a high degree of oxidation (Fig. S8), with ESI− showing the highest average oxygen number of 9.6 oxygen atoms per molecule (Table S3). This is an indicator of acidic functional groups, e.g., hydroxyl (R-OH) or carboxylic acids (R-COOH), which are efficiently ionized by ESI− and lead to the sensitive detection of highly oxidized compounds. High oxygen content is also reflected in a low volatility, which is observed for the wildfire-plume-impacted samples (Fig. 5).

Figure 5. Saturation vapor pressure (C^*) versus m/z plot for unique compounds from averaged wildfire-impacted samples (N01–N05), separated by compound class (black: CHO, blue: CHNO, red: CHOS, green: CHNOS). Compounds abundant after strong wildfire impact (samples N08–N10) are in grey. The aromaticity index is indicated by the dot shape and size. The relative number of compounds per volatility class is listed below each volatility class label.

Van Krevelen (VK) plots (Fig. 4B) show a wide distribution over several structure regions, including the lipid-, phenol-, and carbohydrate-like regions, as well as oxidized aromatic compounds. All of them are known from the literature to be regions of products of biomass burning and atmospheric aging of BB emissions (refer to BB VK). They are not found in PM samples from Nadym (N08–N10) collected after the plume has passed (Fig. S10). ESI− in particular shows intense distribution of signals in the center of the VK plot (medium H/C and O/C), while in each polarity the lipid region of low-oxidized compounds is highly populated. Both regions show no high abundant peaks after 8 August 2021, indicating no significant contribution of fresh biomass burning emissions to ambient PM. Typical elemental compositions of BB markers are found in the wildfire-plume-affected PM samples from Nadym: levoglucosan and its isomeric anhydrosugars, resin acids, methoxyphenols, and lipids. Figure S9 shows semi-quantitative time trends (normalized to the sampling volume) of six biomass burning marker elemental compositions, including elemental compositions of known cellulose and lignin degradation products. The thermal degradation of cellulose structures leads to the formation of the anhydrosugar levoglucosan as well as minor amounts of its isomers galactosan and mannosan. Coniferyl alcohol is a gymnosperm lignin degradation product found, e.g., in pine wood smoke (Simoneit et al., 1993). 7-Oxodehydroabietic acid is emitted from the burning of gymnosperm plants, e.g., Scots pine and larch, which are the dominant forest types in Yakutia (Kharuk et al., 2021). Nonacosene and nonacosanol are biomarkers emitted from higher plant waxes (Simoneit and Elias, 2000). A clear, similar trend is visible for each marker compound, as the abundance increased with a maximum on 7 August 2021 (N04), followed by a slow decrease to 0 towards the end of the observed wildfire plume impact

(9 August 2021). Finally, some peaks are detected in the lower VK space with H/C < 0.7 and 0.2 < O/C < 1.5, particularly in mass spectra of APPI and ESI−. This has been assigned to HU-HOMs, which are produced from the photooxidation of larger PAHs on soot particles, thus indicating heterogeneous processing of wildfire aerosol particles. The formation of HU-HOM changes the polarity of soot particles from hydrophobic to hydrophilic and therefore affects the uptake of water and cloud formation (Li et al., 2022).

The maximum carbonyl ratio (MCR) is a tool used to predict the possible maximum of carbonyl groups in molecules, based on the identification of elemental compositions (Y. Zhang et al., 2021). The applied ionization techniques display differences in the distribution of relative intensity into the five defined MCR areas (Table S4). ESI+ data indicate that there are manifold combinations of oxygen-containing functional groups including not only carbonyl but also single-bound oxygen as found in hydroxyl (R-OH), hydroperoxyl (R-OOH) or ether (R-O-R), which is part of this organic aerosol, as there is a relatively even distribution of compounds for each MCR limit. Comparing the wildfire-plume-affected samples (N01 to N07) with after-plume samples (N08–N10), it is apparent that the distribution of the MCR of samples N08–N10 is shifted to lower MCR, indicating a stronger influence of products from oxidative atmospheric aging. This trend is observed for all applied ionization techniques and may be explained by the lower concentrations of VOCs and thus lower reactivity towards atmospheric oxidants, which lead to more oxidized aging products due to a higher ratio of oxidants to organic carbon compared to dense wildfire plumes.

3.4.2 CHNO

Wildfires, particularly under flaming conditions, are known to emit reactive nitrogen species like nitrogen oxides (NO_x) and nitrous acid (HONO) (Peng et al., 2021; Lindaas et al., 2021). These short-lived compounds may consequently be converted to long-lived peroxyacetyl nitrate (PAN), nitric acid (HNO_3), organic nitrates, or other organic nitrogen-containing compounds (Peng et al., 2021).

PAN and NO_x. take part in atmospheric aging reactions, forming organic aerosol molecules containing the elements oxygen and nitrogen. The most common functional groups are nitrate, nitro, and nitrooxy moieties. Nitrogen-containing compounds are also a relevant portion of BrC due to their potential light-absorbing properties, especially in combination with aromatic ring systems (e.g., nitrophenol derivatives) (Fleming et al., 2020).

The CHON class is the second-most abundant class by intensity but has the highest number of detected compounds in PM affected by wildfires in Nadym, with molecules commonly containing one or two nitrogen atoms. Most compounds of the CHON class show a high degree of oxidation, comparable to the CHO class, with the same shift to a lower oxygen number for ESI+ (Fig. S8). Notably, the oxygen distribution of the ESI− data shows the maximum at nine oxygen atoms, independent of the nitrogen number. An O/N ratio ≥ 3 is the limit for the potential presence of an organic nitrate group, but as the elemental compositions show a high degree of oxidation (O/N $\gg 3$), the detection of hydrocarbons with only nitrate groups is rather unlikely.

Nitroorganics are a relevant species regarding their light-absorption properties and their role in BrC (Salvador et al., 2021). More likely, the majority of compounds detected by ESI and APPI contains more than one functional group, and therefore no clear identifications solely based on the O/N ratio are possible. On the other hand, compounds with an O/N < 3 can be identified as potential nitro compounds, which are frequently detected here by ESI+ (998) and APPI (390).

ESI+ also detects a number of compounds with more or equal amounts of nitrogen compared to oxygen. These compounds could be assigned to alkaloid-like structures or other moieties that include nitrogen-containing heterocyclic compounds (Laskin et al., 2009), which are preferably released under low-temperature and oxygen-poor combustion conditions (Ren and Zhao, 2015).

3.4.3 Sulfur-containing compounds (CHOS/CHNOS)

Sulfur is, to some degree, a part of biomass, e.g., as disulfide bonds or in certain amino acids, and compounds containing sulfur are therefore emitted by biomass burning. Second, e.g., organosulfates are markers for secondary organic aerosol formation with reactions of precursors with anthropogenic pollutants, including sulfates, dimethyl sulfide, and other sulfur-containing nucleophiles like SO_2 (He et al., 2014; Ye et al., 2021). Additionally, marine biogenic emissions of reduced sulfur compounds are a major source of dimethyl sulfide (DMS), carbon disulfide (CS_2), and their oxidation product carbonyl sulfide (OCS) (Qu et al., 2021; Lennartz et al., 2017). The presence of nitrogen in the precursor, as well as the high abundance of NO_x, may also lead to the formation of nitrooxy-organosulfates (He et al., 2014).

CHOS compounds, observed almost exclusively by ESI−, display 4 to 11 oxygen atoms (Fig. S8) as well as low DBE values, indicating long-chain aliphatic structures with one sulfate group and additional oxygen-containing groups. Identical sum formulae have previously been observed in aerosol samples from Chinese megacities (Wang et al., 2016), as well as the ozonolysis of isoprene SOA in the presence of acidic sulfate aerosol (Riva et al., 2016). For example, the CHO_6S_1 class is dominated by one homologous series (DBE = 2) reaching from $C_5H_{10}O_6S_1$ (198.01981 Da) to $C_{35}H_{64}O_6S_1$ (612.44236 Da), including several sum formulae known from the literature, with a proposed terpene origin and the structure of an aliphatic chain with one sulfate, hydroxyl, and carbonyl group each (Riva et al., 2016). Only a few compounds display higher DBE values (DBE = 7), indicating the minor abundance of aromatic precursors. Some of these CHOS compounds are also found in the Nadym PM samples after the plume has passed (N08–N10) but less often and only at higher molecular weights. This may be explained by an independent source of acidic sulfate aerosols, e.g., originating from sea spray or marine emission sources (M. Zhang et al., 2021), leading to the formation of the observed compounds through reactions with biogenic emitted terpenes, e.g., via the epoxide pathway, as well as the presence of other sulfur-containing functional groups, apart from sulfates, like sulfides or thiophenes.

Nitrooxy-organosulfates are also observed in the wildfire-plume-impacted samples (N01–N05) but with a lower relative intensity compared to CHOS compounds (Fig. S11). These compounds are, for example, a product of the combination of two aging reactions adding a nitrate (or nitrooxy) and a sulfate group to one molecule. The sum formulae of one exemplary compound $C_{10}H_{17}N_1O_7S_1$ are suggested to contain one nitrate and one sulfate group, within several isomers, and were also identified in aerosol samples from Shanghai and nighttime oxidation experiments of monoterpenes under acidic conditions (Wang et al., 2016; Surratt et al., 2008). In addition, the sulfur content in CHNOS compounds can also be in the form of sulfides, sulfones, sulfur in ring systems, or other functional groups (Ditto et al., 2021). Detected CHNOS compounds in the main plume are almost exclusively comprised of ELVOC or ULVOC. Similar results for low-volatility CHNOS compounds in aerosol over agricultural fields were linked to a biogenic origin with formation based on sulfate addition to epoxide CHON precursors (Vandergrift et al., 2022).

3.4.4 Reduced compounds (CH/CHN)

Pure hydrocarbons are only detected by APPI due to the poor ionization efficiency of non-polar molecules with ESI, as well as the good ionization efficiency of photoionization for most hydrocarbons (Kauppila et al., 2017). It is expected that hydrocarbons are not found in high abundance in an aged, long-range-transported wildfire plume, as oxidation reactions lead to the transformation of pure hydrocarbons or non-oxygen-containing species. Nevertheless, due to the plume optical thickness protecting hydrocarbons from photolysis and general oxidant deficits, some hydrocarbons are observed, including an extensive homologous series of alkenes from C_{15} to C_{33}. (DBE = 1) as well as higher aromatic structures potentially identified as alkylated (aromatic) ring systems (DBE = 6–9).
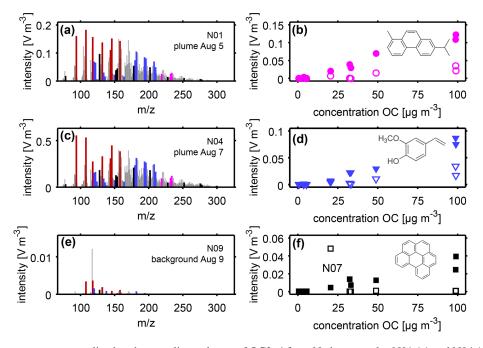
Reduced nitrogen compounds are only found in ESI+, which indicates amine, pyridine, or other basic aromatic nitrogen moieties in the detected molecules. They are found in the moderate DBE range of 4–8, so the occurrence of aromatic structures is possible. Proposed alkaloid structures, in the same DBE range, also containing two or more nitrogen atoms in one molecule, are a known product of incomplete biomass burning, e.g., due to high concentrations in ponderosa pine foliage and thermal stability of these compounds (Laskin et al., 2009).

3.5 Carbohydrate, lignin, and resinoic acid thermal degradation products in PM of Nadym

The REMPI mass spectra from OC fractions OC1 and OC2 were combined to form OC1–2 (Fig. 6), which is dominated by thermal desorption, and OC3 and OC4 to form OC3–4, showing a shift towards smaller molecular masses due to thermal decomposition of larger chemical structures as a complementary approach to FT-ICR MS. As discussed in Sect. 3.4.1 regarding CHO species, BB releases monomers from the decomposition of the biopolymers cellulose, hemicellulose, and lignin, which are commonly used as BB markers. However, the detection of lignans, such as tetrahydro-3,4-divanillylfuran, suggests that phenolic dimers and larger thermal lignin fragments are also emitted (Oros and Simoneit, 2001). Those larger fragments resist the temperatures in OC1–2 but decompose in situ to monomers in OC3–4, which indirectly allows for BB identification. Previous studies have described REMPI mass spectra from the pyrolysis of cellulose, softwood-derived lignin (Grabowsky et al., 2011), several types of biomass (Fendt et al., 2012; Fendt et al., 2013), and SOA from ozonolysis of β-pinene (Diab et al., 2015). Due to the highly oxidized nature of cellulose and SOA, thermal decomposition is similar and complicates the assignment of the mass spectrometric pattern.

All samples which are strongly affected by the wildfire plume exhibit a minimum uncentered correlation coefficient of 0.94. This is in agreement with the similar air mass trajectories to Nadym arriving from 5 to 7 August 2021, while the similarity to the background days is only 0.71 on average. During pyrolysis of low-volatility oxygenated compounds, oxygenated aromatic species are formed, such as phenol (m/z 94), cresol (m/z 108), benzofuran (m/z 118), and naphthols (m/z 144, m/z 158). Hence, most abundant peaks mainly belong to m/z found in OC3 of cellulose and SOA. The pyrolysis yield of lignin-derived species depends on the type of biomass: gymnosperm, angiosperm, or grasses. Although central Yakutia is largely covered by coniferous plants like larch and pine (Kharuk et al., 2021), m/z of syringol-type methoxyphenols (syringaldehyde, m/z 182; allylsyringol, m/z 194; sinapyaldehyde, m/z 208) from angiosperm can be detected next to guaiacol-type methoxyphenols from gymnosperm (guaiacol, m/z 124; methylguaiacol, m/z 138; eugenol, m/z 164; coniferyl alcohol, m/z 180). Moreover, hydroxyphenols from the decomposition of less lignified plants or plant material (B. Simoneit, 2002) are present in the REMPI mass spectra (vinylphenol, m/z 120; dimethylphenol, m/z 122; cinnamic alcohol, m/z 134; anisaldehyde, m/z 136).

In addition to monoaromatic compounds, polycyclic aromatic hydrocarbons and their derivatives are present in the sample or formed in situ. Retene or 1-methyl-7-isopropyl phenanthrene refers to an established marker for the combustion of coniferous biomass (Ramdahl, 1983). It is formed from the thermal degradation of diterpenoids with abietane skeleton. For pine and Siberian larch, most abundant diterpenoids are abietic acid and isopimaric acid as well as levopimaric and palustric acid, respectively (Bardyshev et al., 1970). Their thermal degradation depends on the individual combustion conditions and involves successive dehydrogenation, dealkylation, and decarboxylation, finally resulting in an aromatization of one to three six rings. Consequently, a broad product spectrum is obtained with retene as the most likely reaction product (Standley and Simoneit, 1994; Marchand-Geneste and Carpy, 2003), which has recently been investigated with TOCA-REMPI-TOFMS for spruce logwood and brown coal briquette combustion (Martens et al., 2023). Despite being an alkylated PAH, retene gives a relatively low yield of the molecular ion and partially fragments during REMPI, causing dehydrogenation and demethylation to m/z 232 and m/z 219, respectively. In OC3–4, retene (m/z 234) is formed in situ from earlier thermal degradation products of diterpenoids, such as dehydroabietic acid or simonellite, and highly correlates with the total OC concentrations in Nadym (Fig. 6b), giving evidence for a dominating OC source of burning coniferous biomass. In OC1–2, containing retene, which is truly in the sample, a correlation can also be observed. However, intensities of m/z 234 in OC1–2 are apparently lower than for OC3–4. Primary retene (RET$_{prim}$), which has been formed during combustion and is detected in OC1–2, is associated with more efficient combustion than pyrolytic retene (RET$_{pyr}$), which is formed from the pyrolysis of diterpenoids and their alter-
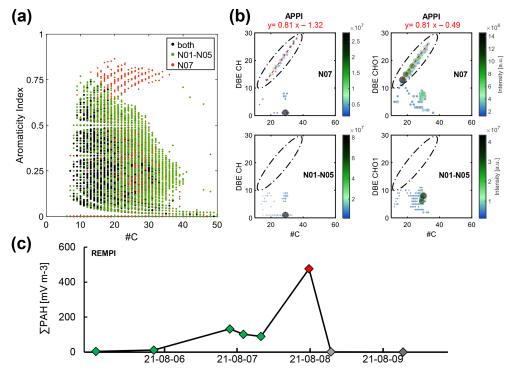
Figure 6. REMPI mass spectra, normalized to the sampling volume, of OC3–4 from Nadym samples N01 **(a)** and N04 **(c)** with elevated OC and EC concentrations as well as N09 as a reference for PM without wildfire impact **(e)**. The different colors indicate decomposition products typical for coniferous plants (magenta), cellulose/SOA (red), and lignin (blue) as well as parent PAH (black). Correlations of **(b)** m/z 234 (e.g., retene), **(d)** m/z 150 (e.g., vinylguaiacol), and **(f)** m/z 276 (e.g., benzo[g,h,i]perylene) in OC1–2 (open symbols) and OC3–4 (filled symbols) to OC.

ation products and is detected in OC3–4. Hence, the ratio of primary retene to total retene (RET_{tot}) in OC may provide a metric for the combustion efficiency of coniferous biomass, similar to the modified combustion efficiency based on CO and CO_2 (Yokelson et al., 1996), which is further evaluated in Sect. S4.

According to RET_{prim}/RET_{tot} close to 0, samples N01–N02 (6 August 2021) contain biomass burning aerosol, e.g., originating from fires under smoldering conditions (Fig. 6). From 7 August 2021 to the morning of 8 August 2021 (N03–N07), the fires became more intense and changed to more flaming conditions, suggested by increased OC and EC concentrations, lower ratios of OC to EC that are typical for higher combustion efficiency, and RET_{prim}/RET_{tot} between 0.15 and 0.26; on these days, the main plume by means of the highest aerosol concentrations arrived in Nadym. During the reference days with typical background concentrations, 1 to 3 orders of magnitude lower intensities for RET_{pyr} and no RET_{prim} were detected, indicating low biomass burning activity. The same approach could be principally used for lignin-derived methoxyphenols, such as vinylguaiacol (m/z 150) (Fig. 6d), but it will be more affected by the dilution because of their higher volatility. Beyond methoxyphenols and retene, REMPI is particularly sensitive to PAH (Streibel and Zimmermann, 2014). In OC3–4, two- to four-ring PAHs (m/z 128, m/z 154, m/z 166, m/z 178, m/z 202, m/z 228) are formed by pyrolysis, but larger PAHs with five or

more aromatic rings (m/z 252, m/z 276, m/z 278, m/z 300, m/z 302) are divided between OC1–2 and OC3–4 (Diab et al., 2015). For m/z 276, representing six-ring PAHs like benzo[g,h,i]perylene or indeno[c,d]pyrene, a good correlation can also be observed with OC (Fig. 6f). However, in OC vs m/z 276 of OC1–2, an outlier emerged, belonging to sample N07. The impact of regional gas flaring and associated emission of PAH is separately discussed in Sect. 3.6.

To estimate the influence of the wildfire plume on ambient particle composition and concentration, a REMPI spectrum of OC3–4 from sample N09 (9 August 2021) with OC and EC concentrations below 1 µg m^{-3}, typical for the Arctic region average (Yasunari et al., 2021), is shown (Fig. 6e). More than 2 orders of magnitude lower intensities were found for lignin-related m/z and 1 order of magnitude lower intensities for aromatics formed from pyrolysis of low-volatility oxygenated compounds. Due to the absence of RET_{pyr}, we conclude that those ions belong to pyrolysis of SOA rather than fragments of carbohydrates. The base peak at m/z 117, however, belongs to indole, which has a 32–40 higher photoionization cross section at 266 nm than toluene (Gehm et al., 2018) and results from the pyrolysis of bioaerosol components, such as proteins (Fuentes et al., 2010), which emphasizes the higher contribution of the natural background to the PM composition in Nadym.
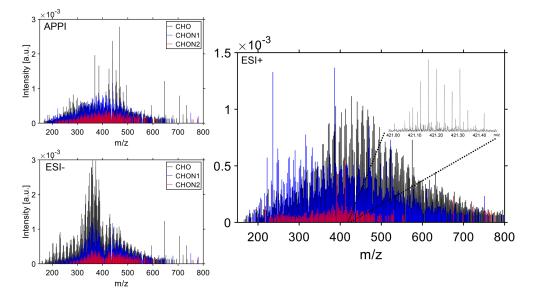
Figure 7. (a) Aromaticity index (AI) versus carbon number plot of sum formulae (APPI) observed uniquely in the wildfire-impacted samples in Nadym (N01–N05, green), in sample N07 additionally impacted by gas flaring (red), or both datasets (black). **(b)** Double-bond equivalent (DBE) versus carbon number plot of CH (left) and CHO_1 (right) compound classes for main plume (bottom) and N07 (top) with the linear equation of the planar limit indicated in red. **(c)** Time trend of summed intensities of parent-PAH-related m/z (128, 152, 178, 202, 228, 252, 276, 278, 300, and 302) detected by TOCA-REMPI-TOFMS in OC1–2.

3.6 Impact of gas flaring on PM composition in Nadym

In addition to long-range-transported wildfire emissions, gas flaring from open excess-gas burning at oil and gas fields is one of the major sources of black carbon (BC) emissions in the Siberian Arctic (Popovicheva et al., 2022, 2017; Stohl et al., 2013). Sample N07 was not apparent in OC and EC compared to the other wildfire-plume-impacted samples (N05 and N08) collected on the days before and afterward but differed in chemical composition. Backward air mass trajectories for sample N07 show the transport of air masses through the region south of Nadym, where many oil and gas fields are located (Fig. S2). A unique pattern of compounds is observed in both APPI-FT-ICR MS and TOCA-REMPI MS, with each ionization technique being sensitive to the detection of aromatic hydrocarbon compounds due to the favorable photoionization properties of aromatic ring structures (Gehm et al., 2018; Huba et al., 2016). When excess gaseous organic compounds are burned in a gas flare, incomplete combustion can lead, among others, to the formation of aromatic hydrocarbons in a large range of molecular sizes, from benzene to aromatic soot precursors with large condensed ring structures in various structural combinations and sizes (Slavinskaya and Frank, 2009; T. Zhang et al., 2021; Senkan, 1996). Figure 7a shows a comparison

of averaged samples impacted by the wildfire plume (N01–N05) and sample N07 APPI data, highlighting unique, condensed aromatic compounds (AI > 0.67), with up to 40 carbon atoms, exclusively observed in N07. Due to their pyrogenic formation, no pronounced alkylation is observed in these compounds, which is a key factor for the differentiation to condensed aromatic structures, e.g., found in petroleum (Fig. 7b). By calculating the slope of the planar limit and the ratio of core to methylated species intensity ($C_0/C_0 + C_1$) in the sample N07 (Fig. 7b, Table S5), the pyrogenic origin (slope: 0.81, $C_0/C_0 + C_1$: 0.7–0.8) is confirmed (Yunker et al., 2002; Cho et al., 2011). A slope of the planar limit from 0.75 to 1 indicates the addition of benzene rings linearly or nonlinearly to a core structure, and a maximum of intensity for each DBE value at C_0 is associated with combustion emissions (Laflamme and Hites, 1978).

As pointed out in Sect. 3.5, markers of BB in the TOCA-REMPI mass spectrum of OC34 strongly correlate with the total content of OC. However, for m/z of PAH, such as m/z 276 representing six-ring PAHs, sample N07 of 8 August 2021 deviates from this correlation (Fig. 6f). In the REMPI mass spectrum of OC12, minor fragments at m/z 118, 132, and 146 from low-temperature pyrolysis of carbohydrates and SOA are visible, but larger parent PAHs dominate the mass spectrum of N07 in contrast to wildfire plume

Figure 8. TIC normalized mass spectra of assigned CHO (black), $CHON_1$ (blue), and $CHON_2$ (red) elemental compositions identified in the wildfire-affected PM sampled at Bely Island, collected by APPI and ESI during the period during which wildfire aerosol arrived in Nadym. Zoomed-in representation of one nominal mass of the ESI+ spectrum, highlighting the molecular complexity of oxygenated compounds at m/z 421.

sample N03 (Fig. S12) and support the findings from APPI-FT-ICR MS.

Despite apparent differences in air mass trajectories of sample N07, containing PM from long-range-transported wildfire plume, from N05 or N08, the mass spectrometric analyses suggest the presence of a high-temperature combustion aerosol, such as from gas flaring, which was added to the chemical PM signature of biomass burning and aged organic aerosol. Both wildfire and gas flaring can be regarded as the most significant contributors to PM in northern Siberia.

3.7 Chemical characterization of PM from Bely Island

FT-ICR MS data of wildfire plume that affect PM on Bely Island, collected during the same period of high PM levels in Nadym (sample B01, 31 July to 6 August 2021), show a similar or even higher complexity than the PM in Nadym as well as partly different chemical composition. Figure 8 shows mass spectra of the three most abundant compound classes in the range of m/z 150–800 in APPI and ESI, with APPI showing approximately the same number of identified sum formulae (5231), ESI− showing a lower number (3553), and ESI+ showing even more identified formulae (7361) in PM on Bely Island (B01) compared to the composition of PM in Nadym averaged from 5 to 8 August 2021 (N01 to N07). When comparing the spectra of Fig. 8 with data from Nadym (Fig. S13), differences in the chemical composition become apparent.

The most pronounced region in the APPI spectrum of Nadym PM samples affected by wildfire plume (N01–N07) is m/z 400–500, containing high intensities of CHO1–

CHO4 compounds with moderate aromaticity (DBE 5–10). This section is less abundant in the mass spectrum from PM of Bely Island (B01), but the lower m/z region compounds (200–350 Da), including CHO5–CHO7, are more pronounced. The same shift to a higher degree of oxidation can be observed in the ESI+ data of the PM samples from Bely Island. The CHO8–CHO14 compounds compile the broad signal distribution of the CHO class at m/z 400–800 in the PM samples from Bely Island, while the ESI+ spectrum of Nadym PM samples is characterized by single intense signals of, e.g., marker compound masses like levoglucosan, which is not identified on Bely Island, and a more equal distribution of the remaining majority of signals.

The lower abundance of biomass burning marker compounds in PM samples from Bely Island could be attributed to more pronounced aging and SOA formation of the air masses reaching the Arctic region, reducing the amount of primary biomass burning markers.

In the REMPI mass spectra of OC3–4, BB-related thermal fragments discussed in Sect. 3.5 are clearly visible for the weekly samples from 31 July to 7 August 2021 (B01) and from 7 to 14 August 2021 (B02) (Fig. S14a and b). However, compared to a main plume sample from Nadym (N05) (Fig. S14d), these samples from Bely show distinct higher m/z in OC3–4, possibly due to the formation of larger, chemically different or more stable structures. The ratio of RET_{pyr} to OC in B01 and B02 is 30 % to 50 % lower than in sample N05 but still confirms the significant contribution of BB aerosol. In the sample after the plume event from 14 to 21 August 2021 (B03), both overall and BB-related thermal fragments disappeared in the REMPI mass spectrum,

Table 1. Sum parameter trends comparing wildfire plume datasets from Nadym and Bely Island of the same period (31 July to 7 August 2021; "<": increase, "≈": steady, ">": decrease).

Nadym → Bely	APPI			ESI−			ESI+		
	Nadym		Bely Island	Nadym		Bely Island	Nadym		Bely Island
AI < 0.25 [% int.]	55.60	<	66.45	69.22	<	75.96	86.09	<	88.56
AI > 0.5 [% int.]	6.83	>	4.48	2.71	<	3.40	0.87	<	2.12
DBE	8.07	>	7.09	7.70	>	6.75	5.28	<	6.01
OS_C	−0.80	<	−0.61	−0.50	<	−0.32	−1.09	<	−0.78
$\log(C^*)$	−5.41	<	−5.19	−8.01	<	−4.99	−5.49	≈	−5.87
O/C	0.31	<	0.42	0.48	<	0.54	0.30	<	0.40
O/N	5.78	<	6.65	6.66	<	8.39	4.70	<	6.83
CHO [% int.]	47.12	<	48.10	44.05	<	64.70	45.96	<	51.40
CHNO [% int.]	47.76	>	44.10	36.71	>	28.60	47.38	>	45.30

while N-containing thermal fragments from the degradation of bioaerosol components, such as from proteins, increased in relative abundance at m/z 117 (indole) and m/z 131 (methylindole) (Fig. 139C) (Fuentes et al., 2010).

When comparing sum parameters determined from the elemental composition assignment of both datasets (Tables 1, S3, S6, and S7), a trend resulting from an increased photochemical age is visible. All ionization techniques show that the samples collected on Bely Island are more oxidized and less aromatic with a higher saturation vapor pressure, as well as higher average O/C and O/N ratios. The relative CHO intensity is increased, while the other relative intensities are decreased. AAE values are also decreased, indicating degradation of chromophores by photobleaching (Liu et al., 2021). This behavior indicates more intense atmospheric aging, especially by reactions adding oxygen to the organic aerosol molecules, but not nitrogen or sulfur. This is contrary to observations made for the evolution of emissions from a boreal forest fire in Lac La Loche (Canada), where an increase in nitrogen- and also sulfur-containing compounds was observed (Ditto et al., 2021). The lower concentrations from the wildfire plume periphery result in a higher ratio of atmospheric oxidants to reactive aerosol constituents. Furthermore, the more remote location of Bely Island compared to Nadym determines a lower mixing with reactive gases from anthropogenic emissions (e.g., NO_x and SO_x). Therefore, the PM composition in Bely Island shows a picture of more intensively oxidized organic matter with a lower content of N- and S-containing compounds compared to PM from Nadym.

For a molecular insight into the differences in PM composition in Nadym and on Bely Island, the intersect of both datasets in each ionization technique is determined (Fig. 9a). The compound class distribution of each section gives an overview of the chemical composition unique to each sampling location. A large fraction of sum formulae is present in both datasets, which is explained by the almost-identical source of the PM emissions. Nevertheless, a high number of compounds is uniquely abundant in one of the two datasets.

The m/z unique to Nadym PM contains a disproportionate number of nitrogen-containing compounds (CHNO), while the PM sample from Bely Island contains more CHO compounds (except for APPI) relative to CHON compounds.
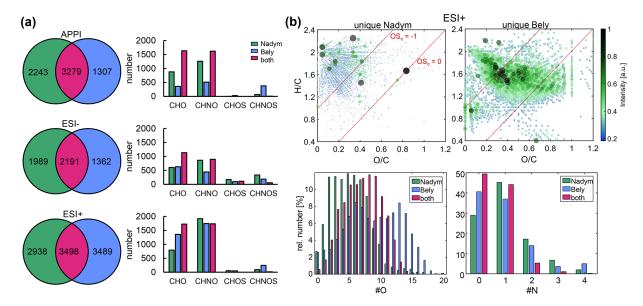
Van Krevelen plots of all applied ionization techniques reveal a clearly visible difference in the fingerprint of unique organic compounds (Fig. 9). Peaks only detected in the Nadym PM are in the low to medium O/C range, with a H/C ratio larger than 1.2 and an average $OS_C < −1$. On the other hand, unique peaks in PM of Bely Island show a much higher O/C range, with abundant average OS_C in the range of −1 to 0, as well as abundant low O/C and low H/C compounds.

The number of unique nitrogen-containing compounds is almost identical for both sites, but the relative nitrogen number distribution is shifted to lower (or 0) nitrogen numbers for PM of Bely Island. An opposite trend is observed for the oxygen number distribution. The unique peaks detected in PM from Bely Island show a much higher degree of oxygenation (maximum at 13 oxygen atoms), whereas most of the unique peaks in Nadym PM samples contain less than 6 oxygen atoms. The overlap of both datasets is observed in between both oxygen number distributions.
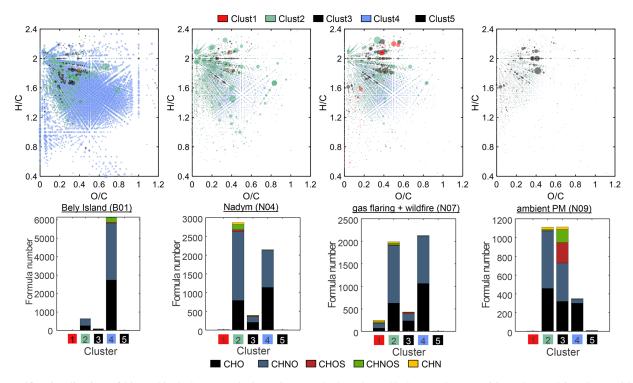
These characteristic differences between wildfire plume PM in Nadym and on Bely Island agree with the previously discussed more intensive atmospheric aging of the organic aerosol in wildfire PM collected on Bely Island compared to the relatively fresh aerosol collected in Nadym.

3.8 Elucidation the origin of individual elemental compositions by hierarchical clustering

Hierarchical cluster analysis is applied to better understand which compounds of the tens of thousands of identified elemental compositions are the most relevant for the characterization and differentiation of the observed sample origins (wildfire plumes sampled in Nadym and on Bely Island, mixing of plume with gas flaring emissions, and samples after the wildfire plume had passed). Considering all elemental compositions, including both [M+H] and [M+Na] adducts

Figure 9. (a) Venn diagram with sum formula numbers (left) and relative intensity compound class distributions (right) of Nadym main plume (green) and Bely Island (blue) wildfire aerosol datasets. **(b)** Van Krevelen plot of unique compounds (ESI+) identified in Nadym and on Bely Island PM samples and relative number distribution of oxygen- and nitrogen-containing compounds for unique and shared (magenta) elemental compositions.

Figure 10. Visualization of hierarchical cluster analysis (HCA) results based on all elemental compositions detected in ESI+, with the number of clusters set to five. Van Krevelen (VK) plots of four exemplary samples and bar plots of the compound class distribution in each cluster. The colors in the VK plot indicate the cluster assignment of each elemental composition, with dot size indicating the intensity of each compound. Cluster 4 (blue) is associated with aged wildfire compounds, cluster 2 (green) is associated with fresher wildfire aerosol, cluster 1 (red) is associated with gas flaring, and cluster 3 and cluster 5 (black) are associated with ambient PM without a contribution of wildfires on Bely Island and in Nadym, respectively.

that are found in ESI+ datasets, HCA (with a maximum number of clusters set to five) is performed to sort each elemental composition into a separate cluster (average silhouette value = 0.40) (Merder et al., 2021). The resulting clustergram (Fig. S15) shows the grouping of samples with a known similar origin into the same clusters. In order to highlight molecules related to different sample origins, the elemental composition clustering results are summarized into five main clusters. The chemical characteristics of the results are visualized in Van Krevelen space and compound class distribution plots (Fig. 10).

The analysis of elemental compositions by HCA emphasizes the dominating influence of wildfire emissions on the complex chemical composition of the detected organic aerosol species. Compounds present in the ambient aerosol samples are also observed as a constant background in the PM samples affected by wildfires at both sampling sites. The clustering in combination with knowledge of the respective dominating emission sources for each sample allows for a deeper discussion of the identified clusters.

Compounds of cluster 4 are detected with high abundance (intensity and number) in the wildfire-affected PM on Bely Island but are also, less dominating, present in the Nadym PM samples with wildfire influence (Fig. S16). The VK plot (Fig. 10) shows a broad distribution of compounds with O/C ratios up to unity. The complex pattern shown by these compounds is in line with the previous finding of intensively aged biomass burning aerosol arriving at Bely Island from 31 July to 6 August 2021. Cluster 2 contains typical compounds present in wildfire-affected PM sampled in Nadym, which are rarely present in PM on Bely Island with and without wildfire influence. The pattern shown by compounds in this cluster is less distributed over the VK space, with lower O/C ratios and higher H/C ratios, compared to the SOA compounds in cluster 4. This suggests less intense atmospheric aging of the wildfire plume arriving in Nadym from 5 to 8 August 2021; thus PM in Nadym was still substantial and had a clear signature of fresh biomass burning emissions. In addition to the fresh biomass burning emissions, aged aerosol species (cluster 4) are also detected. The detection of both aged and fresh biomass burning emissions agrees with the observation of higher aerosol absorption in the part of the wildfire plume transported to Nadym than that transported to Bely Island. A high wildfire plume density suppresses photochemistry inside of the plume due to light absorption, lower OH radical production, and a lower ratio of atmospheric oxidants to reactive aerosol species. Therefore, cluster 2 and 4 contain similar numbers of sum formulae in PM samples affected by wildfire aerosol in Nadym but substantially more sum formulae in cluster 4 in PM samples affected by wildfires on Bely Island.

The impact of gas flaring on sample N07 is clearly represented by compounds in cluster 1 (red), as it is the only sample where cluster 1 is significantly populated. Compounds of this cluster are found in the highly aromatic, low-O/C-ratio region of the VK space, as has previously been discussed for the gas-flaring-impacted sample. Compounds from typical concentration levels in Nadym and on Bely Island, termed ambient aerosol samples (N08–N10 and B03), are grouped into clusters 3 and 5, respectively. Cluster 5 makes its highest contribution to the Bely sample without wildfire impact, while compounds from cluster 3 are found in most PM samples of Nadym with the highest relative contribution after the wildfire plume had passed the site.

4 Conclusions

Our study shows the long-range transportation of wildfire plume over different trajectories and provides insights into the chemical composition of aged air pollutants in the Siberian Arctic. Due to PM sampling in Nadym and on Bely Island in the north of western Siberia at the same time, it was possible to observe the different atmospheric fates of the plume periphery and center aerosol at similar atmospheric residence times and transport distances. First, back-trajectory analysis with in-depth chemical characterization of the organic compounds through complementary mass spectrometric techniques revealed a complex organic mixture of primary and secondary organic aerosols at both sites and confirmed the dominant biomass burning source for samples N01 to N07. In situ detection of resinoic acids and alteration products as pyrolytic retene in relation to primary retene specified the biomass to coniferous vegetation and possibly provides an additional indication of the combustion efficiency in biomass burning. Furthermore, the additional influence of regional gas flaring on sample N07 could be underlined from its contribution of larger PAHs to the PM burden, which may serve as a criterion to separate contributions to the Arctic PM burden by wildfire from anthropogenic combustion emissions. After the plume passed Nadym, neither the molecular signature of BB nor gas flaring was found in samples N08 to N10, with up to 1 order of magnitude lower concentrations of OC and EC compared to samples N01 to N07.

During the main plume period at both sites, CHO and CHON were the dominating compound classes observed in ultra-high-resolution mass spectra by all ionization techniques, with especially nitrogen-containing compounds being of interest due to their effect on the light-absorbing properties of aerosols. Nevertheless, both sites showed distinct differences in their more detailed chemical properties. PM samples from Bely Island were more oxidized with a higher oxidation state but lower aromaticity than PM samples from Nadym. The biomass burning aerosol arriving at Bely Island was identified as originating from the plume periphery of lower concentration; thus it underwent more intense atmospheric aging than the center plume transported to Nadym, despite similar physical plume ages. Finally, hierarchical clustering of the ultra-high-resolution mass spectra from ESI+ could sort the detected sum formulae and decon-

volute the chemical composition according to contributing aerosol sources.

The long-range transport of a wildfire plume from central Siberia was observed as an intense event of carbonaceous aerosol influx to the vulnerable Arctic ecosystem. Typical ambient concentrations of OC and EC in Nadym and on Bely Island were exceeded by 1 to 2 orders of magnitude. Moreover, $AAE_{405/808}$ from 1.5 to 3.3 suggested the presence of BrC in Nadym, but the weekly average of $AAE_{405/808}$ over a similar period on Bely Island accounted for 1–1.2, indicating more intense atmospheric aging and degradation of BrC chromophores from the same wildfire plume.

Despite the known impact of wildfire plumes on the Arctic aerosol composition, the investigated PM samples from Nadym and Bely Island describe a long-range-transport event with unprecedented high concentrations of carbonaceous aerosol. Detailed chemical characterization of aged wildfire aerosol emissions provides insights into biomass burning and atmospheric processes and may improve our understanding of interactions between the biosphere and atmosphere as well as consequences on the Arctic ecosystem and climate.

Author contributions. ES: methodology, investigation, formal analysis, writing (original draft), visualization; HC: conceptualization, investigation, formal analysis, writing (original draft), visualization, supervision, project administration; OP: conceptualization, investigation, data curation, writing (original draft), supervision, project administration, funding acquisition; VK: data curation, resources, writing (review and editing); MC: software, formal analysis, visualization, writing (review and editing); NK: investigation, writing (review and editing); TM: investigation, writing (review and editing); CPR: methodology, software, resources, writing (review and editing), supervision, project administration; RZ: resources, writing (review and editing), funding acquisition.

References

Abatzoglou, J. T., Williams, A. P., and Barbero, R.: Global Emergence of Anthropogenic Climate Change in Fire Weather Indices, Geophys. Res. Lett., 46, 326–336, https://doi.org/10.1029/2018GL080959, 2019.

Al-Abadleh, H. A.: Aging of atmospheric aerosols and the role of iron in catalyzing brown carbon formation, Environ. Sci. Atmos., 1, 297–345, https://doi.org/10.1039/D1EA00038A, 2021.

Andreae, M. O. and Gelencsér, A.: Black carbon or brown carbon? The nature of light-absorbing carbonaceous aerosols, Atmos. Chem. Phys., 6, 3131–3148, https://doi.org/10.5194/acp-6-3131-2006, 2006.

Bardyshev, I. I., Kryuk, S. I., and Pertsovskii, A. L.: Fatty acid composition of various balsams and rosins, Chem. Nat. Compd., 6, 360–361, https://doi.org/10.1007/BF00567321, 1970.

Bond, T. C., Doherty, S. J., Fahey, D. W., Forster, P. M., Berntsen, T., DeAngelo, B. J., Flanner, M. G., Ghan, S., Kärcher, B., Koch, D., Kinne, S., Kondo, Y., Quinn, P. K., Sarofim, M. C., Schultz, M. G., Schulz, M., Venkataraman, C., Zhang, H., Zhang, S., Bellouin, N., Guttikunda, S. K., Hopke, P. K., Jacobson, M. Z., Kaiser, J. W., Klimont, Z., Lohmann, U., Schwarz, J. P., Shindell, D., Storelvmo, T., Warren, S. G., and Zender, C. S.: Bounding the role of black carbon in the climate system: A

scientific assessment, Geophys. Res. Atmos., 118, 5380–5552, https://doi.org/10.1002/jgrd.50171, 2013.

Brege, M. A., China, S., Schum, S., Zelenyuk, A., and Mazzoleni, L. R.: Extreme Molecular Complexity Resulting in a Continuum of Carbonaceous Species in Biomass Burning Tar Balls from Wildfire Smoke, ACS Earth Space Chem., 5, 2729–2739, https://doi.org/10.1021/acsearthspacechem.1c00141, 2021.

Calì Quaglia, F., Meloni, D., Muscari, G., Di Iorio, T., Ciardini, V., Pace, G., Becagli, S., Di Bernardino, A., Cacciani, M., Hannigan, J. W., Ortega, I., and Di Sarra, A. G.: On the Radiative Impact of Biomass-Burning Aerosols in the Arctic: The August 2017 Case Study, Remote Sens.-Basel, 14, 313, https://doi.org/10.3390/rs14020313, 2022.

Chacon-Madrid, H. J. and Donahue, N. M.: Fragmentation vs. functionalization: chemical aging and organic aerosol formation, Atmos. Chem. Phys., 11, 10553–10563, https://doi.org/10.5194/acp-11-10553-2011, 2011.

Chakrabarty, R. K., Moosmüller, H., Chen, L.-W. A., Lewis, K., Arnott, W. P., Mazzoleni, C., Dubey, M. K., Wold, C. E., Hao, W. M., and Kreidenweis, S. M.: Brown carbon in tar balls from smoldering biomass combustion, Atmos. Chem. Phys., 10, 6363–6370, https://doi.org/10.5194/acp-10-6363-2010, 2010.

Chen, G., Guo, Y., Yue, X., Tong, S., Gasparrini, A., Bell, M. L., Armstrong, B., Schwartz, J., Jaakkola, J. J. K., Zanobetti, A., Lavigne, E., Nascimento Saldiva, P. H., Kan, H., Royé, D., Milojevic, A., Overcenco, A., Urban, A., Schneider, A., Entezari, A., Vicedo-Cabrera, A. M., Zeka, A., Tobias, A., Nunes, B., Alahmad, B., Forsberg, B., Pan, S.-C., Íñiguez, C., Ameling, C., La Cruz Valencia, C. de, Åström, C., Houthuijs, D., van Dung, D., Samoli, E., Mayvaneh, F., Sera, F., Carrasco-Escobar, G., Lei, Y., Orru, H., Kim, H., Holobaca, I.-H., Kyselý, J., Teixeira, J. P., Madureira, J., Katsouyanni, K., Hurtado-Díaz, M., Maasikmets, M., Ragettli, M. S., Hashizume, M., Stafoggia, M., Pascal, M., Scortichini, M., Sousa Zanotti Stagliorio Coêlho, M. de, Valdés Ortega, N., Ryti, N. R. I., Scovronick, N., Matus, P., Goodman, P., Garland, R. M., Abrutzky, R., Garcia, S. O., Rao, S., Fratianni, S., Dang, T. N., Colistro, V., Huber, V., Lee, W., Seposo, X., Honda, Y., Guo, Y. L., Ye, T., Yu, W., Abramson, M. J., Samet, J. M., and Li, S.: Mortality risk attributable to wildfire-related PM$_{2.5}$ pollution: a global time series study in 749 locations, Lancet Planetary Health, 5, e579-e587, https://doi.org/10.1016/S2542-5196(21)00200-X, 2021.

Chen, L.-W. A., Moosmüller, H., Arnott, W. P., Chow, J. C., Watson, J. G., Susott, R. A., Babbitt, R. E., Wold, C. E., Lincoln, E. N., and Hao, W. M.: Particle emissions from laboratory combustion of wildland fuels: In situ optical and mass measurements, Geophys. Res. Lett., 33, L04803, https://doi.org/10.1029/2005GL024838, 2006.

Chen, L.-W. A., Chow, J. C., Wang, X. L., Robles, J. A., Sumlin, B. J., Lowenthal, D. H., Zimmermann, R., and Watson, J. G.: Multi-wavelength optical measurement to enhance thermal/optical analysis for carbonaceous aerosol, Atmos. Meas. Tech., 8, 451–461, https://doi.org/10.5194/amt-8-451-2015, 2015.

Cheng, Y., Duan, F., He, K., Zheng, M., Du, Z., Ma, Y., and Tan, J.: Intercomparison of thermal-optical methods for the determination of organic and elemental carbon: influences of aerosol composition and implications, Environ. Sci. Technol., 45, 10117–10123, https://doi.org/10.1021/es202649g, 2011.

Cho, Y., Kim, Y. H., and Kim, S.: Planar limit-assisted structural interpretation of saturates/aromatics/resins/asphaltenes fractionated crude oil compounds observed by Fourier transform ion cyclotron resonance mass spectrometry, Anal. Chem., 83, 6068–6073, https://doi.org/10.1021/ac2011685, 2011.

Chow, J. C., Watson, J. G., Chen, L. W. A., Chang, M. C. O., Robinson, N. F., Trimble, D., and Kohl, S.: The IMPROVE_A temperature protocol for thermal/optical carbon analysis: maintaining consistency with a long-term database, J. Air Waste Manage. Assoc. (1995), 57, 1014–1023, https://doi.org/10.3155/1047-3289.57.9.1014, 2007.

Chow, J. C., Chen, L.-W. A., Wang, X., Green, M. C., and Watson, J. G.: Improved estimation of PM$_{2.5}$ brown carbon contributions to filter light attenuation, Particuology, 56, 1–9, https://doi.org/10.1016/j.partic.2021.01.001, 2021.

Decker, Z. C. J., Robinson, M. A., Barsanti, K. C., Bourgeois, I., Coggon, M. M., DiGangi, J. P., Diskin, G. S., Flocke, F. M., Franchin, A., Fredrickson, C. D., Gkatzelis, G. I., Hall, S. R., Halliday, H., Holmes, C. D., Huey, L. G., Lee, Y. R., Lindaas, J., Middlebrook, A. M., Montzka, D. D., Moore, R., Neuman, J. A., Nowak, J. B., Palm, B. B., Peischl, J., Piel, F., Rickly, P. S., Rollins, A. W., Ryerson, T. B., Schwantes, R. H., Sekimoto, K., Thornhill, L., Thornton, J. A., Tyndall, G. S., Ullmann, K., Van Rooy, P., Veres, P. R., Warneke, C., Washenfelder, R. A., Weinheimer, A. J., Wiggins, E., Winstead, E., Wisthaler, A., Womack, C., and Brown, S. S.: Nighttime and daytime dark oxidation chemistry in wildfire plumes: an observation and model analysis of FIREX-AQ aircraft data, Atmos. Chem. Phys., 21, 16293–16317, https://doi.org/10.5194/acp-21-16293-2021, 2021.

Diab, J., Streibel, T., Cavalli, F., Lee, S. C., Saathoff, H., Mamakos, A., Chow, J. C., Chen, L.-W. A., Watson, J. G., Sippula, O., and Zimmermann, R.: Hyphenation of a EC / OC thermal–optical carbon analyzer to photo-ionization time-of-flight mass spectrometry: an off-line aerosol mass spectrometric approach for characterization of primary and secondary particulate matter, Atmos. Meas. Tech., 8, 3337–3353, https://doi.org/10.5194/amt-8-3337-2015, 2015.

Ditto, J. C., He, M., Hass-Mitchell, T. N., Moussa, S. G., Hayden, K., Li, S.-M., Liggio, J., Leithead, A., Lee, P., Wheeler, M. J., Wentzell, J. J. B., and Gentner, D. R.: Atmospheric evolution of emissions from a boreal forest fire: the formation of highly functionalized oxygen-, nitrogen-, and sulfur-containing organic compounds, Atmos. Chem. Phys., 21, 255–267, https://doi.org/10.5194/acp-21-255-2021, 2021.

Donahue, N. M., Epstein, S. A., Pandis, S. N., and Robinson, A. L.: A two-dimensional volatility basis set: 1. organic-aerosol mixing thermodynamics, Atmos. Chem. Phys., 11, 3303–3318, https://doi.org/10.5194/acp-11-3303-2011, 2011.

Donahue, N. M., Kroll, J. H., Pandis, S. N., and Robinson, A. L.: A two-dimensional volatility basis set – Part 2: Diagnostics of organic-aerosol evolution, Atmos. Chem. Phys., 12, 615–634, https://doi.org/10.5194/acp-12-615-2012, 2012.

Eleftheriadis, K., Nyeki, S., Psomiadou, C., and Colbeck, I.: Background Aerosol Properties in the European Arctic, Water Air Soil Pollut. Focus, 4, 23–30, https://doi.org/10.1023/B:WAFO.0000044783.70114.19, 2004.

Fang, Z., Li, C., He, Q., Czech, H., Gröger, T., Zeng, J., Fang, H., Xiao, S., Pardo, M., Hartner, E., Meidan, D., Wang, X., Zimmermann, R., Laskin, A., and Rudich, Y.: Secondary organic aerosols

produced from photochemical oxidation of secondarily evaporated biomass burning organic gases: Chemical composition, toxicity, optical properties, and climate effect, Environ. Int., 157, 106801, https://doi.org/10.1016/j.envint.2021.106801, 2021.

Farley, R., Bernays, N., Jaffe, D. A., Ketcherside, D., Hu, L., Zhou, S., Collier, S., and Zhang, Q.: Persistent Influence of Wildfire Emissions in the Western United States and Characteristics of Aged Biomass Burning Organic Aerosols under Clean Air Conditions, Environ. Sci. Technol., 56, 3645–3657, https://doi.org/10.1021/acs.est.1c07301, 2022.

Fendt, A., Streibel, T., Sklorz, M., Richter, D., Dahmen, N., and Zimmermann, R.: On-Line Process Analysis of Biomass Flash Pyrolysis Gases Enabled by Soft Photoionization Mass Spectrometry, Energy Fuels, 26, 701–711, https://doi.org/10.1021/ef2012613, 2012.

Fendt, A., Geissler, R., Streibel, T., Sklorz, M., and Zimmermann, R.: Hyphenation of two simultaneously employed soft photo ionization mass spectrometers with thermal analysis of biomass and biochar, Thermochim. Acta, 551, 155–163, https://doi.org/10.1016/j.tca.2012.10.002, 2013.

Flannigan, M. D., Krawchuk, M. A., Groot, W. J. de, Wotton, B. M., and Gowman, L. M.: Implications of changing climate for global wildland fire, Int. J. Wildland Fire, 18, 483, https://doi.org/10.1071/WF08187, 2009.

Fleming, L. T., Lin, P., Roberts, J. M., Selimovic, V., Yokelson, R., Laskin, J., Laskin, A., and Nizkorodov, S. A.: Molecular composition and photochemical lifetimes of brown carbon chromophores in biomass burning organic aerosol, Atmos. Chem. Phys., 20, 1105–1129, https://doi.org/10.5194/acp-20-1105-2020, 2020.

Forrister, H., Liu, J., Scheuer, E., Dibb, J., Ziemba, L., Thornhill, K. L., Anderson, B., Diskin, G., Perring, A. E., Schwarz, J. P., Campuzano-Jost, P., Day, D. A., Palm, B. B., Jimenez, J. L., Nenes, A., and Weber, R. J.: Evolution of brown carbon in wildfire plumes, Geophys. Res. Lett., 42, 4623–4630, https://doi.org/10.1002/2015GL063897, 2015.

Fuentes, M., Baigorri, R., González-Vila, F. J., González-Gaitano, G., and García-Mina, J. M.: Pyrolysis-gas chromatography/mass spectrometry identification of distinctive structures providing humic character to organic materials, J. Environ. Qual., 39, 1486–1497, https://doi.org/10.2134/jeq2009.0180, 2010.

Gehm, C., Streibel, T., Passig, J., and Zimmermann, R.: Determination of Relative Ionization Cross Sections for Resonance Enhanced Multiphoton Ionization of Polycyclic Aromatic Hydrocarbons, Appl. Sci.-Basel, 8, 1617, https://doi.org/10.3390/app8091617, 2018.

Grabowsky, J., Streibel, T., Sklorz, M., Chow, J. C., Watson, J. G., Mamakos, A., and Zimmermann, R.: Hyphenation of a carbon analyzer to photo-ionization mass spectrometry to unravel the organic composition of particulate matter on a molecular level, Anal. Bioanal. Chem., 401, 3153–3164, https://doi.org/10.1007/s00216-011-5425-1, 2011.

He, Q.-F., Ding, X., Wang, X.-M., Yu, J.-Z., Fu, X.-X., Liu, T.-Y., Zhang, Z., Xue, J., Chen, D.-H., Zhong, L.-J., and Donahue, N. M.: Organosulfates from pinene and isoprene over the Pearl River Delta, South China: seasonal variation and implication in formation mechanisms, Environ. Sci. Technol., 48, 9236–9245, https://doi.org/10.1021/es501299v, 2014.

Helin, A., Virkkula, A., Backman, J., Pirjola, L., Sippula, O., Aakko-Saksa, P., Väätäinen, S., Mylläri, F., Järvinen, A., Bloss, M., Aurela, M., Jakobi, G., Karjalainen, P., Zimmermann, R., Jokiniemi, J., Saarikoski, S., Tissari, J., Rönkkö, T., Niemi, J. V., and Timonen, H.: Variation of Absorption Ångström Exponent in Aerosols From Different Emission Sources, Geophys. Res. Atmos., 126, https://doi.org/10.1029/2020JD034094, 2021.

Hodshire, A. L., Ramnarine, E., Akherati, A., Alvarado, M. L., Farmer, D. K., Jathar, S. H., Kreidenweis, S. M., Lonsdale, C. R., Onasch, T. B., Springston, S. R., Wang, J., Wang, Y., Kleinman, L. I., Sedlacek III, A. J., and Pierce, J. R.: Dilution impacts on smoke aging: evidence in Biomass Burning Observation Project (BBOP) data, Atmos. Chem. Phys., 21, 6839–6855, https://doi.org/10.5194/acp-21-6839-2021, 2021.

Huba, A. K., Huba, K., and Gardinali, P. R.: Understanding the atmospheric pressure ionization of petroleum components: The effects of size, structure, and presence of heteroatoms, Sci. Total Environ., 568, 1018–1025, https://doi.org/10.1016/j.scitotenv.2016.06.044, 2016.

Ikeda, K. and Tanimoto, H.: Exceedances of air quality standard level of $PM_{2.5}$ in Japan caused by Siberian wildfires, Environ. Res. Lett., 10, 105001, https://doi.org/10.1088/1748-9326/10/10/105001, 2015.

IPCC: Climate Change 2013: The Physical Science Basis. Contribution of Working Group I to the Fifth Assessment Report of the Intergovernmental Panel on Climate Change, edited by: Stocker, T. F., Qin, D., Plattner, G.-K., Tignor, M., Allen, S. K., Boschung, J., Nauels, A., Xia, Y., Bex, V., and Midgley, P. M., Cambridge University Press, Cambridge, United Kingdom and New York, NY, USA, 1535 pp., https://doi.org/10.1017/CBO9781107415324, 2013.

Kalogridis, A.-C., Popovicheva, O. B., Engling, G., Diapouli, E., Kawamura, K., Tachibana, E., Ono, K., Kozlov, V. S., and Eleftheriadis, K.: Smoke aerosol chemistry and aging of Siberian biomass burning emissions in a large aerosol chamber, Atmos. Environ., 185, 15–28, https://doi.org/10.1016/j.atmosenv.2018.04.033, 2018.

Kauppila, T. J., Syage, J. A., and Benter, T.: Recent developments in atmospheric pressure photoionization-mass spectrometry, Mass Spectrom. Rev., 36, 423–449, https://doi.org/10.1002/mas.21477, 2017.

Kharuk, V. I., Ponomarev, E. I., Ivanova, G. A., Dvinskaya, M. L., Coogan, S. C. P., and Flannigan, M. D.: Wildfires in the Siberian taiga, Ambio, 50, 1953–1974, https://doi.org/10.1007/s13280-020-01490-x, 2021.

Laflamme, R. E. and Hites, R. A.: The global distribution of polycyclic aromatic hydrocarbons in recent sediments, Geochim. Cosmochim. Ac., 42, 289–303, https://doi.org/10.1016/0016-7037(78)90182-5, 1978.

Laskin, A., Smith, J. S., and Laskin, J.: Molecular characterization of nitrogen-containing organic compounds in biomass burning aerosols using high-resolution mass spectrometry, Environ. Sci. Technol., 43, 3764–3771, https://doi.org/10.1021/es803456n, 2009.

Lavoué, D., Liousse, C., Cachier, H., Stocks, B. J., and Goldammer, J. G.: Modeling of carbonaceous particles emitted by boreal and temperate wildfires at northern latitudes, Geophys. Res. Atmos., 105, 26871–26890, https://doi.org/10.1029/2000JD900180, 2000.

Lee, J. E., Dubey, M. K., Aiken, A. C., Chylek, P., and Carrico, C. M.: Optical and Chemical Analysis of Absorption Enhancement by Mixed Carbonaceous Aerosols in the 2019 Woodbury, AZ, Fire Plume, Geophys. Res. Atmos., 125, https://doi.org/10.1029/2020JD032399, 2020.

Lennartz, S. T., Marandino, C. A., von Hobe, M., Cortes, P., Quack, B., Simo, R., Booge, D., Pozzer, A., Steinhoff, T., Arevalo-Martinez, D. L., Kloss, C., Bracher, A., Röttgers, R., Atlas, E., and Krüger, K.: Direct oceanic emissions unlikely to account for the missing source of atmospheric carbonyl sulfide, Atmos. Chem. Phys., 17, 385–402, https://doi.org/10.5194/acp-17-385-2017, 2017.

Li, C., He, Q., Hettiyadura, A. P. S., Käfer, U., Shmul, G., Meidan, D., Zimmermann, R., Brown, S. S., George, C., Laskin, A., and Rudich, Y.: Formation of Secondary Brown Carbon in Biomass Burning Aerosol Proxies through NO3 Radical Reactions, Environ. Sci. Technol., 54, 1395–1405, https://doi.org/10.1021/acs.est.9b05641, 2020.

Li, M., Li, J., Zhu, Y., Chen, J., Andreae, M. O., Pöschl, U., Su, H., Kulmala, M., Chen, C., Cheng, Y., and Zhao, J.: Highly oxygenated organic molecules with high unsaturation formed upon photochemical aging of soot, Chem, 8, 2688–2699, https://doi.org/10.1016/j.chempr.2022.06.011, 2022.

Lin, P., Liu, J., Shilling, J. E., Kathmann, S. M., Laskin, J., and Laskin, A.: Molecular characterization of brown carbon (BrC) chromophores in secondary organic aerosol generated from photo-oxidation of toluene, Phys. Chem. Chem. Phys., 17, 23312–23325, https://doi.org/10.1039/C5CP02563J, 2015.

Lindaas, J., Pollack, I. B., Garofalo, L. A., Pothier, M. A., Farmer, D. K., Kreidenweis, S. M., Campos, T. L., Flocke, F., Weinheimer, A. J., Montzka, D. D., Tyndall, G. S., Palm, B. B., Peng, Q., Thornton, J. A., Permar, W., Wielgasz, C., Hu, L., Ottmar, R. D., Restaino, J. C., Hudak, A. T., Ku, I.-T., Zhou, Y., Sive, B. C., Sullivan, A., Collett, J. L., and Fischer, E. V.: Emissions of Reactive Nitrogen From Western U. S. Wildfires During Summer 2018, J. Geophys. Res.-Atmos., 126, https://doi.org/10.1029/2020JD032657, 2021.

Liu, D., Li, S., Hu, D., Kong, S., Cheng, Y., Wu, Y., Ding, S., Hu, K., Zheng, S., Yan, Q., Zheng, H., Zhao, D., Tian, P., Ye, J., Huang, M., and Ding, D.: Evolution of Aerosol Optical Properties from Wood Smoke in Real Atmosphere Influenced by Burning Phase and Solar Radiation, Environ. Sci. Technol., 55, 5677–5688, https://doi.org/10.1021/acs.est.0c07569, 2021.

Manousakas, M., Popovicheva, O., Evangeliou, N., Diapouli, E., Sitnikov, N., Shonija, N., and Eleftheriadis, K.: Aerosol carbonaceous, elemental and ionic composition variability and origin at the Siberian High Arctic, Cape Baranova, Tellus B, 72, 1803708, https://doi.org/10.1080/16000889.2020.1803708, 2022.

Marchand-Geneste, N. and Carpy, A.: Theoretical study of the thermal degradation pathways of abietane skeleton diterpenoids: aromatization to retene, J. Mol. Struct.-THEOCHEM, 635, 55–82, https://doi.org/10.1016/S0166-1280(03)00401-9, 2003.

Martens, P., Czech, H., Orasche, J., Abbaszade, G., Sklorz, M., Michalke, B., Tissari, J., Bizjak, T., Ihalainen, M., Suhonen, H., Yli-Pirilä, P., Jokiniemi, J., Sippula, O., and Zimmermann, R.: Brown Coal and Logwood Combustion in a Modern Heating Appliance: The Impact of Combustion Quality and Fuel on Organic Aerosol Composition, Environ. Sci. Technol., 57, 5532–5543, https://doi.org/10.1021/acs.est.2c08787, 2023.

Matsui, H., Mori, T., Ohata, S., Moteki, N., Oshima, N., Goto-Azuma, K., Koike, M., and Kondo, Y.: Contrasting source contributions of Arctic black carbon to atmospheric concentrations, deposition flux, and atmospheric and snow radiative effects, Atmos. Chem. Phys., 22, 8989–9009, https://doi.org/10.5194/acp-22-8989-2022, 2022.

Merder, J., Röder, H., Dittmar, T., Feudel, U., Freund, J. A., Gerdts, G., Kraberg, A., and Niggemann, J.: Dissolved organic compounds with synchronous dynamics share chemical properties and origin, Limnol. Oceanogr., 66, 4001–4016, https://doi.org/10.1002/lno.11938, 2021.

MODIS Science Team: MOD021KM MODIS/Terra Calibrated Radiances 5-Min L1B Swath 1 km, NASA [data set], 2017a.

MODIS Science Team: MOD02HKM MODIS/Terra Calibrated Radiances 5-Min L1B Swath 500 m, NASA [data set], 2017b.

MODIS Science Team: MOD02QKM MODIS/Terra Calibrated Radiances 5-Min L1B Swath 250 m, NASA [data set], 2017c.

MODIS Science Team: MYD02QKM MODIS/Aqua Calibrated Radiances 5-Min L1B Swath 250 m, NASA [data set], 2017d.

Moschos, V., Dzepina, K., Bhattu, D., Lamkaddam, H., Casotto, R., Daellenbach, K. R., Canonaco, F., Rai, P., Aas, W., Becagli, S., Calzolai, G., Eleftheriadis, K., Moffett, C. E., Schnelle-Kreis, J., Severi, M., Sharma, S., Skov, H., Vestenius, M., Zhang, W., Hakola, H., Hellén, H., Huang, L., Jaffrezo, J.-L., Massling, A., Nøjgaard, J. K., Petäjä, T., Popovicheva, O., Sheesley, R. J., Traversi, R., Yttri, K. E., Schmale, J., Prévôt, A. S. H., Baltensperger, U., and El Haddad, I.: Equal abundance of summertime natural and wintertime anthropogenic Arctic organic aerosols, Nat. Geosci., 15, 196–202, https://doi.org/10.1038/s41561-021-00891-1, 2022.

Narita, D., Gavrilyeva, T., and Isaev, A.: Impacts and management of forest fires in the Republic of Sakha, Russia: A local perspective for a global problem, Polar Sci., 27, 100573, https://doi.org/10.1016/j.polar.2020.100573, 2021.

NASA: VIIRS and MODIS, NASA Earthdata [data set], https://www.earthdata.nasa.gov/ (last access: 3 April 2023), 2023.

NUR24.RU: Смог от пожаров в Якутии полностью окутал Ямал (ФОТО, ВИДЕО), Gorodor, https://nur24.ru/news/ecologia/smog-ot-pozharov-v-yakutii-polnostyu-okutal-yamal-foto-video (last access: 7 February 2023), 2021.

Oros, D. R. and Simoneit, B. R.: Identification and emission factors of molecular tracers in organic aerosols from biomass burning Part 2. Deciduous trees, Appl. Geochem., 16, 1545–1565, https://doi.org/10.1016/S0883-2927(01)00022-1, 2001.

Ortega, A. M., Day, D. A., Cubison, M. J., Brune, W. H., Bon, D., de Gouw, J. A., and Jimenez, J. L.: Secondary organic aerosol formation and primary organic aerosol oxidation from biomass-burning smoke in a flow reactor during FLAME-3, Atmos. Chem. Phys., 13, 11551–11571, https://doi.org/10.5194/acp-13-11551-2013, 2013.

Palm, B. B., Peng, Q., Fredrickson, C. D., Lee, B. H., Garofalo, L. A., Pothier, M. A., Kreidenweis, S. M., Farmer, D. K., Pokhrel, R. P., Shen, Y., Murphy, S. M., Permar, W., Hu, L., Campos, T. L., Hall, S. R., Ullmann, K., Zhang, X., Flocke, F., Fischer, E. V., and Thornton, J. A.: Quantification of organic aerosol and brown carbon evolution in fresh wildfire plumes, P. Natl. Acad. Sci. USA, 117, 29469–29477, https://doi.org/10.1073/pnas.2012218117, 2020.

Palm, B. B., Peng, Q., Hall, S. R., Ullmann, K., Campos, T. L., Weinheimer, A., Montzka, D., Tyndall, G., Permar, W., Hu, L., Flocke, F., Fischer, E. V., and Thornton, J. A.: Spatially Resolved Photochemistry Impacts Emissions Estimates in Fresh Wildfire Plumes, Geophys. Res. Lett., 48, https://doi.org/10.1029/2021GL095443, 2021.

Pardo, M., Offer, S., Hartner, E., Di Bucchianico, S., Bisig, C., Bauer, S., Pantzke, J., Zimmermann, E. J., Cao, X., Binder, S., Kuhn, E., Huber, A., Jeong, S., Käfer, U., Schneider, E., Mesceriakovas, A., Bendl, J., Brejcha, R., Buchholz, A., Gat, D., Hohaus, T., Rastak, N., Karg, E., Jakobi, G., Kalberer, M., Kanashova, T., Hu, Y., Ogris, C., Marsico, A., Theis, F., Shalit, T., Gröger, T., Rüger, C. P., Oeder, S., Orasche, J., Paul, A., Ziehm, T., Zhang, Z.-H., Adam, T., Sippula, O., Sklorz, M., Schnelle-Kreis, J., Czech, H., Kiendler-Scharr, A., Zimmermann, R., and Rudich, Y.: Exposure to naphthalene and β-pinene-derived secondary organic aerosol induced divergent changes in transcript levels of BEAS-2B cells, Environ. Int., 166, 107366, https://doi.org/10.1016/j.envint.2022.107366, 2022.

Peng, Q., Palm, B. B., Fredrickson, C. D., Lee, B. H., Hall, S. R., Ullmann, K., Campos, T., Weinheimer, A. J., Apel, E. C., Flocke, F., Permar, W., Hu, L., Garofalo, L. A., Pothier, M. A., Farmer, D. K., Ku, I.-T., Sullivan, A. P., Collett, J. L., Fischer, E., and Thornton, J. A.: Observations and Modeling of NO x Photochemistry and Fate in Fresh Wildfire Plumes, ACS Earth Space Chem., 5, 2652–2667, https://doi.org/10.1021/acsearthspacechem.1c00086, 2021.

Popovicheva, O. and Kozlov, V.: Impact of combustion phase on scattering and spectral absorption of Siberian biomass burning: studies in Large Aerosol Chamber, 252, Proceedings Volume 11560, 26th International Symposium on Atmospheric and Ocean Optics, Atmospheric Physics, 115604N, https://doi.org/10.1117/12.2575583, 2020.

Popovicheva, O., Diapouli, E., Makshtas, A., Shonija, N., Manousakas, M., Saraga, D., Uttal, T., and Eleftheriadis, K.: East Siberian Arctic background and black carbon polluted aerosols at HMO Tiksi, Sci. Total Environ., 655, 924–938, https://doi.org/10.1016/j.scitotenv.2018.11.165, 2019.

Popovicheva, O. B., Kozlov, V. S., Engling, G., Diapouli, E., Persiantseva, N. M., Timofeev, M. A., Fan, T.-S., Saraga, D., and Eleftheriadis, K.: Small-Scale Study of Siberian Biomass Burning: I. Smoke Microstructure, Aerosol Air Qual. Res., 15, 117–128, https://doi.org/10.4209/aaqr.2014.09.0206, 2015.

Popovicheva, O. B., Kozlov, V. S., Rakhimov, R. F., Shmargunov, V. P., Kireeva, E. D., Persiantseva, N. M., Timofeev, M. A., Engling, G., Eleftheriadis, K., Diapouli, E., Panchenko, M. V., Zimmermann, R., and Schnelle-Kreis, J.: Optical-microphysical and physical-chemical characteristics of Siberian biomass burning: Experiments in Aerosol Chamber, Atmos. Oceanic Opt., 29, 492–500, https://doi.org/10.1134/S1024856016060129, 2016.

Popovicheva, O. B., Evangeliou, N., Eleftheriadis, K., Kalogridis, A. C., Sitnikov, N., Eckhardt, S., and Stohl, A.: Black Carbon Sources Constrained by Observations in the Russian High Arctic, Environ. Sci. Technol., 51, 3871–3879, https://doi.org/10.1021/acs.est.6b05832, 2017.

Popovicheva, O. B., Chichaeva, M., Kobelev, V., Sinitskiy, A., and Hansen, A.: Black Carbon in urban emissions on the Polar Circle, 344, Proceedings Volume 11560, 26th International Symposium on Atmospheric and Ocean Optics, Atmo-spheric Physics, 115605J, https://doi.org/10.1117/12.2577550, https://www.spiedigitallibrary.org/conference-proceedings-of-spie/11560/2577550/Black-Carbon-in-urban-emissions-on-the-Polar-Circle/10.1117/12.2577550.full (last access: 3 February 2023), 2020.

Popovicheva, O. B., Evangeliou, N., Kobelev, V. O., Chichaeva, M. A., Eleftheriadis, K., Gregorič, A., and Kasimov, N. S.: Siberian Arctic black carbon: gas flaring and wildfire impact, Atmos. Chem. Phys., 22, 5983–6000, https://doi.org/10.5194/acp-22-5983-2022, 2022.

Popovicheva, O. B., Chichaeva, M. A., Kobelev, V. O., and Kasimov, N. S.: Black Carbon Seasonal Trends and Regional Sources on Bely Island (Arctic), Atmos. Oceanic Opt., 36, 176–184, https://doi.org/10.1134/S1024856023030090, 2023.

QGIS: Geographical information for the creation of maps, QGIS [data set], https://qgis.org/en/site/ (last access: 3 April 2023), 2023.

Qu, B., Gabric, A. J., and Jackson, R.: Simulated perturbation in the sea-to-air flux of dimethylsulfide and the impact on polar climate, J. Oceanol. Limnol., 39, 110–121, https://doi.org/10.1007/s00343-020-0007-8, 2021.

Ramdahl, T.: Retene—a molecular marker of wood combustion in ambient air, Nature, 306, 580–582, https://doi.org/10.1038/306580a0, 1983.

Ren, Q. and Zhao, C.: Evolution of fuel-N in gas phase during biomass pyrolysis, Renew. Sust. Energ. Rev., 50, 408–418, https://doi.org/10.1016/j.rser.2015.05.043, 2015.

Riva, M., Budisulistiorini, S. H., Zhang, Z., Gold, A., and Surratt, J. D.: Chemical characterization of secondary organic aerosol constituents from isoprene ozonolysis in the presence of acidic aerosol, Atmos. Environ., 130, 5–13, https://doi.org/10.1016/j.atmosenv.2015.06.027, 2016.

Rüger, C. P., Schwemer, T., Sklorz, M., O'Connor, P. B., Barrow, M. P., and Zimmermann, R.: Comprehensive chemical comparison of fuel composition and aerosol particles emitted from a ship diesel engine by gas chromatography atmospheric pressure chemical ionisation ultra-high resolution mass spectrometry with improved data processing routines, Eur. J. Mass Spectrom., 23, 28–39, https://doi.org/10.1177/1469066717694286, 2017.

Salvador, C. M. G., Tang, R., Priestley, M., Li, L., Tsiligiannis, E., Le Breton, M., Zhu, W., Zeng, L., Wang, H., Yu, Y., Hu, M., Guo, S., and Hallquist, M.: Ambient nitro-aromatic compounds – biomass burning versus secondary formation in rural China, Atmos. Chem. Phys., 21, 1389–1406, https://doi.org/10.5194/acp-21-1389-2021, 2021.

Schmale, J., Zieger, P., and Ekman, A. M. L.: Aerosols in current and future Arctic climate, Nat. Clim. Change, 11, 95–105, https://doi.org/10.1038/s41558-020-00969-5, 2021.

Schneider, E., Czech, H., Popovicheva, O., Lütdke, H., Schnelle-Kreis, J., Khodzher, T., Rüger, C. P., and Zimmermann, R.: Molecular Characterization of Water-Soluble Aerosol Particle Extracts by Ultrahigh-Resolution Mass Spectrometry: Observation of Industrial Emissions and an Atmospherically Aged Wildfire Plume at Lake Baikal, ACS Earth Space Chem., 6, 1095–1107, https://doi.org/10.1021/acsearthspacechem.2c00017, 2022.

Schnitzler, E. G., Gerrebos, N. G. A., Carter, T. S., Huang, Y., Heald, C. L., Bertram, A. K., and Abbatt, J. P. D.: Rate of atmospheric brown carbon whitening governed by environmen-

tal conditions, P. Natl. Acad. Sci. USA, 119, e2205610119, https://doi.org/10.1073/pnas.2205610119, 2022.

Semoutnikova, E. G., Gorchakov, G. I., Sitnov, S. A., Kopeikin, V. M., Karpov, A. V., Gorchakova, I. A., Ponomareva, T. Y., Isakov, A. A., Gushchin, R. A., Datsenko, O. I., Kurbatov, G. A., and Kuznetsov, G. A.: Siberian Smoke Haze over European Territory of Russia in July 2016: Atmospheric Pollution and Radiative Effects, Atmos. Oceanic Opt., 31, 171–180, https://doi.org/10.1134/S1024856018020124, 2018.

Senkan, S.: Formation of polycyclic aromatic hydrocarbons (PAH) in methane combustion: Comparative new results from premixed flames, Combust. Flame, 107, 141–150, https://doi.org/10.1016/0010-2180(96)00044-2, 1996.

Simoneit, B. R.: Biomass burning — a review of organic tracers for smoke from incomplete combustion, Appl. Geochem., 17, 129–162, https://doi.org/10.1016/S0883-2927(01)00061-0, 2002.

Simoneit, B. R. and Elias, V. O.: Organic tracers from biomass burning in atmospheric particulate matter over the ocean, Mar. Chem., 69, 301–312, https://doi.org/10.1016/S0304-4203(00)00008-6, 2000.

Simoneit, B. R. T., Rogge, W. F., Mazurek, M. A., Standley, L. J., Hildemann, L. M., and Cass, G. R.: Lignin pyrolysis products, lignans, and resin acids as specific tracers of plant classes in emissions from biomass combustion, Environ. Sci. Technol., 27, 2533–2541, https://doi.org/10.1021/es00048a034, 1993.

SkyTruth: Oil and gas flare location data, SkyTruth [data set], https://skytruth.org/ (last access: 3 April 2023), 2023.

Slavinskaya, N. A. and Frank, P.: A modelling study of aromatic soot precursors formation in laminar methane and ethene flames, Combust. Flame, 156, 1705–1722, https://doi.org/10.1016/j.combustflame.2009.04.013, 2009.

Standley, L. J. and Simoneit, B. R. T.: Resin diterpenoids as tracers for biomass combustion aerosols, J. Atmos. Chem., 18, 1–15, https://doi.org/10.1007/BF00694371, 1994.

Stein, A. F., Draxler, R. R., Rolph, G. D., Stunder, B. J. B., Cohen, M. D., and Ngan, F.: NOAA's HYSPLIT Atmospheric Transport and Dispersion Modeling System, B. Am. Meteorol. Soc., 96, 2059–2077, https://doi.org/10.1175/BAMS-D-14-00110.1, 2015.

Stohl, A., Klimont, Z., Eckhardt, S., Kupiainen, K., Shevchenko, V. P., Kopeikin, V. M., and Novigatsky, A. N.: Black carbon in the Arctic: the underestimated role of gas flaring and residential combustion emissions, Atmos. Chem. Phys., 13, 8833–8855, https://doi.org/10.5194/acp-13-8833-2013, 2013.

Streibel, T. and Zimmermann, R.: Resonance-enhanced multiphoton ionization mass spectrometry (REMPI-MS): applications for process analysis, Annu. Rev. Anal. Chem., 7, 361–381, https://doi.org/10.1146/annurev-anchem-062012-092648, 2014.

Surratt, J. D., Gómez-González, Y., Chan, A. W. H., Vermeylen, R., Shahgholi, M., Kleindienst, T. E., Edney, E. O., Offenberg, J. H., Lewandowski, M., Jaoui, M., Maenhaut, W., Claeys, M., Flagan, R. C., and Seinfeld, J. H.: Organosulfate formation in biogenic secondary organic aerosol, J. Phys. Chem. A, 112, 8345–8378, https://doi.org/10.1021/jp802310p, 2008.

Tang, J., Li, J., Su, T., Han, Y., Mo, Y., Jiang, H., Cui, M., Jiang, B., Chen, Y., Tang, J., Song, J., Peng, P., and Zhang, G.: Molecular compositions and optical properties of dissolved brown carbon in biomass burning, coal combustion, and vehicle emission aerosols illuminated by excitation–emission matrix spec-

troscopy and Fourier transform ion cyclotron resonance mass spectrometry analysis, Atmos. Chem. Phys., 20, 2513–2532, https://doi.org/10.5194/acp-20-2513-2020, 2020.

Tomshin, O. A. and Solovyev, V. S.: Detection of burnt areas in Yakutia on long-term NOAA satellites data (1985–2015), Proceedings Volume 10833, 24th International Symposium on Atmospheric and Ocean Optics: Atmospheric Physics, 108338B, 288, https://doi.org/10.1117/12.2504569, 2018.

Torres, O. O.: OMPS-NPP L2 NM Aerosol Index swath orbital, NASA [data set], https://doi.org/10.5067/40L92G8144IV, 2019.

Vandergrift, G. W., Shawon, A. S. M., Dexheimer, D. N., Zawadowicz, M. A., Mei, F., and China, S.: Molecular Characterization of Organosulfate-Dominated Aerosols over Agricultural Fields from the Southern Great Plains by High-Resolution Mass Spectrometry, ACS Earth Space Chem., 6, 1733–1741, https://doi.org/10.1021/acsearthspacechem.2c00043, 2022.

Wang, X. K., Rossignol, S., Ma, Y., Yao, L., Wang, M. Y., Chen, J. M., George, C., and Wang, L.: Molecular characterization of atmospheric particulate organosulfates in three megacities at the middle and lower reaches of the Yangtze River, Atmos. Chem. Phys., 16, 2285–2298, https://doi.org/10.5194/acp-16-2285-2016, 2016.

Watson, J. G. and Chow, J. C.: Comparison and evaluation of in situ and filter carbon measurements at the Fresno Supersite, Geophys. Res. Atmos., 107, ICC 3-1–ICC 3-15, https://doi.org/10.1029/2001JD000573, 2002.

Yasunari, T. J., Nakamura, H., Kim, K.-M., Choi, N., Lee, M.-I., Tachibana, Y., and Da Silva, A. M.: Relationship between circum-Arctic atmospheric wave patterns and large-scale wildfires in boreal summer, Environ. Res. Lett., 16, 64009, https://doi.org/10.1088/1748-9326/abf7ef, 2021.

Ye, Y., Zhan, H., Yu, X., Li, J., Wang, X., and Xie, Z.: Detection of organosulfates and nitrooxy-organosulfates in Arctic and Antarctic atmospheric aerosols, using ultra-high resolution FT-ICR mass spectrometry, Sci. Total Environ., 767, 144339, https://doi.org/10.1016/j.scitotenv.2020.144339, 2021.

Yokelson, R. J., Griffith, D. W. T., and Ward, D. E.: Open-path Fourier transform infrared studies of large-scale laboratory biomass fires, Geophys. Res. Atmos., 101, 21067–21080, https://doi.org/10.1029/96JD01800, 1996.

Yue, S., Zhu, J., Chen, S., Xie, Q., Li, W., Li, L., Ren, H., Su, S., Li, P., Ma, H., Fan, Y., Cheng, B., Wu, L., Deng, J., Hu, W., Ren, L., Wei, L., Zhao, W., Tian, Y., Pan, X., Sun, Y., Wang, Z., Wu, F., Liu, C.-Q., Su, H., Penner, J. E., Pöschl, U., Andreae, M. O., Cheng, Y., and Fu, P.: Brown carbon from biomass burning imposes strong circum-Arctic warming, One Earth, 5, 293–304, https://doi.org/10.1016/j.oneear.2022.02.006, 2022.

Yunker, M. B., Macdonald, R. W., Vingarzan, R., Mitchell, R. H., Goyette, D., and Sylvestre, S.: PAHs in the Fraser River basin: a critical appraisal of PAH ratios as indicators of PAH source and composition, Org. Geochem., 33, 489–515, https://doi.org/10.1016/S0146-6380(02)00002-5, 2002.

Zhang, M., Marandino, C. A., Yan, J., Lin, Q., Park, K., and Xu, G.: DMS sea-to-air fluxes and their influence on sulfate aerosols over the Southern Ocean, south-east Indian Ocean and north-west Pacific Ocean, Environ. Chem., 18, 193, https://doi.org/10.1071/EN21003, 2021.

Zhang, T., Mu, G., Zhang, S., and Hou, J.: Formation pathways of polycyclic aromatic hydrocarbons (PAHs) in

butane or butadiene flames, RSC Adv., 11, 5629–5642, https://doi.org/10.1039/D0RA08744K, 2021.

Zhang, Y., Wang, K., Tong, H., Huang, R.-J., and Hoffmann, T.: The maximum carbonyl ratio (MCR) as a new index for the structural classification of secondary organic aerosol components, Rapid Commun. Mass Sp., 35, e9113, https://doi.org/10.1002/rcm.9113, 2021.